Journal of Rock Mechanics and Geotechnical Engineering 18 (2026) 3447–3470

Contents lists available at ScienceDirect

Journal of Rock Mechanics and Geotechnical Engineering

journal homepage: www.jrmge.cn

Full Length Article

Thermo-mechanical degradation and crack evolution of granite subjected to liquid nitrogen cooling cycles for thermal reservoir stimulation

Yi Xue [a,b], Linchao Wang [a], Zhengzheng Cao [b,*], Heping Xie [c], P.G. Ranjith [d], Chengzheng Cai [e]

[a] School of Civil Engineering and Architecture, Xi'an University of Technology, Xi'an, 710048, China
[b] State Key Laboratory Cultivation Base for Gas Geology and Gas Control, Henan Polytechnic University, Jiaozuo, 454000, China
[c] Institute of Deep Earth Science and Green Energy, College of Civil and Transportation Engineering, Shenzhen University, Shenzhen, 518052, China
[d] Deep Earth Energy Laboratory, Department of Civil Engineering, Monash University, Melbourne, Victoria, 3800, Australia
[e] State Key Laboratory for Geomechanics and Deep Underground Engineering, China University of Mining and Technology, Xuzhou, 221006, China

ARTICLE INFO

Article history:
Received 25 January 2025
Received in revised form
28 August 2025
Accepted 22 September 2025
Available online 16 December 2025

Keywords:
Liquid nitrogen fracturing
Ultrasound
Fracture behavior
Fracture morphology
Fracture energy

ABSTRACT

Liquid nitrogen (LN_2)-assisted fracturing has emerged as a promising technique to enhance the productivity of hot dry rock (HDR) geothermal reservoirs. To elucidate the progressive mechanical degradation and fracture mechanisms of granite under cyclic thermal shocks, this study integrates ultrasonic testing, acoustic emission (AE) monitoring, three-dimensional profilometry, and uniaxial compression testing. Damage evolution was assessed through velocity attenuation, waveform distortion, and AE characteristics, while microcrack propagation and fracture morphology were analyzed using scanning electron microscopy and surface topography reconstruction. The degradation process exhibits a distinct cycle-dependent transition, evolving from tensile microcrack initiation during early cycles to shear-dominated failure during prolonged cycling. In Phase I (1–3 cycles), initial thermal stresses induce axial tensile microcracks, leading to sharp decreases in P-wave velocity (53.45 %) and amplitude (40.55 %). Frequency analysis reveals a narrowing and convergence of secondary bands, whereas the fracture surfaces exhibit low undulation, dominated by tensile failure. In Phase II (3–20 cycles), shear-dominated damage progressively develops, as cyclic cooling enhances crack connectivity. AE activity intensifies sharply, correlating with macroscopic shear crack networks. Fracture surfaces evolve toward step-like morphologies, with roughness parameters increasing by up to 277.43 %, indicative of composite tensile–shear failure. Cyclic LN_2 cooling significantly lowers crack initiation stress and fracture energy, while promoting crack density and surface roughness. These findings provide critical insights into the mechanisms of LN_2-induced fracture enhancement, highlighting its potential to optimize HDR reservoir stimulation strategies.

1. Introduction

The world today faces two major challenges: growing energy demand and escalating environmental pollution. To ensure sustainable economic development, transitioning from fossil fuels to renewable energy is urgently needed. In this context, geothermal energy from hot dry rock (HDR) has gained increasing global attention due to its abundant reserves, clean nature, and renewable characteristics, positioning it as a critical strategic alternative to fossil fuels (Asai et al., 2022; Hamd-Allah and Al-Ameri, 2023; Wang et al., 2025; Zhu et al., 2025).

HDR reservoirs are typically found at depths of 5–6 km, within high-temperature rock formations (150 °C–650 °C). These formations mainly consist of low-permeability crystalline rocks, such as granite (Breede et al., 2013). The development of these reservoirs relies on Enhanced Geothermal Systems, a process that includes:

* Corresponding author.
E-mail address: caozz@hpu.edu.cn (Z. Cao).

Peer review under responsibility of Institute of Rock and Soil Mechanics, Chinese Academy of Sciences.

https://doi.org/10.1016/j.jrmge.2025.09.019

(1) the establishment of injection and production well networks using directional drilling technology; (2) the construction of fracture networks through thermal stimulation, chemical stimulation, or hydraulic fracturing; and (3) the injection of low-temperature fluids for circulation to extract thermal energy (Hu et al., 2022). However, the high strength, low porosity, and low fracture toughness of granite result in poor frackability (Lu, 2018). Thus, developing complex fracture networks within geothermal reservoirs to enhance thermal conductivity remains a critical challenge. While hydraulic fracturing, as the current mainstream method, can modify reservoirs, it presents several drawbacks: high fracturing pressures are required in hard formations, with substantial water consumption per well, and issues such as wastewater treatment and excessive water resource consumption persist.

Liquid nitrogen (LN_2) fracturing is a novel, waterless technique. It creates a fracture flow network through the dual effects of ultra-low temperature phase change (boiling point at −196.56 °C) and thermal stress. At the laboratory scale, triaxial tests by Qu et al. (2022) and Hong et al. (2022) revealed that, compared to traditional hydraulic fracturing, LN_2 fracturing reduced the initiation pressure by 12.4 %–51.5 %, increased fracture tortuosity by 5.9 %, and formed a multi-branch fracture network. Cha et al. (2021) performed visual experiments using transparent core cylinder samples to observe crack initiation and propagation. They found that horizontal fractures predominated during LN_2 fracturing, and the fracture network became more three-dimensional and complex. These experimental results demonstrate the significant potential of LN_2 fracturing technology for enhancing the modification of HDR reservoirs, offering new possibilities for improving HDR development efficiency.

Numerous laboratory studies have been conducted to examine the fracture and damage effects of LN_2 on high-temperature HDR reservoirs. Research findings indicate that during the use of LN_2-assisted fracturing in HDR, factors such as rock temperature, LN_2 cooling rate, and the number of cooling cycles are closely associated with the resulting thermal damage. For instance, Shao et al. (2022) investigated granite heated to four distinct temperature gradients, followed by LN_2-cooling tests. Their results revealed that surface roughness increases with rising heating temperatures. Below 200 °C, crack resistance slightly improves, whereas above 200 °C, fracture toughness shows a negative correlation with heating temperature. Wang et al. (2024) observed a similar trend. They demonstrated that crack resistance responds in stages to temperature changes, with 200 °C being a critical threshold. Conversely, Ge et al. (2021) suggested that under rapid LN_2 cooling conditions, 400 °C acts as the pivotal temperature threshold, beyond which significant changes occur in the physical, mechanical, and fracture characteristics of granite. When temperatures exceed 400 °C, heat-induced internal damage in granite worsens, enhancing its plastic behavior and substantially reducing fracture toughness. Mahesar et al. (2020) used scanning electron microscopy (SEM) to analyze the impact of LN_2 cooling on the pore structure of sandstone. Their findings revealed that after 90 min of cooling, crack width and connectivity increased significantly, with a 58 % rise in porosity and a 74 % reduction in the nanoindentation modulus. Additionally, the LN_2 cooling rate plays a critical role in the degradation of granite's mechanical properties. Wu et al. (2019), Sha et al. (2020), and Li et al. (2020) performed comprehensive comparisons of thermal damage in rocks at high temperatures, investigating various cooling methods, including air, water, and LN_2 cooling. These studies consistently showed that LN_2 cooling causes the most severe degradation in physical and mechanical properties, compared to air and water cooling. The thermal shock effects become more pronounced as rock temperatures rise. Furthermore, a single cooling cycle often has limited thermal damage and does not significantly enhance rock fracturing efficiency. Therefore, cyclic cooling is commonly employed to lower the rock's fracture initiation pressure and increase fracturing volume. Rong et al. (2021) performed 24 cycles of LN_2 cooling on granite and found that increasing the number of cycles led to a continuous degradation in physical and mechanical properties, including reductions in wave velocity, porosity, and strength. However, after 12 cycles, the extent of damage stabilized. Similarly, Ge and Sun (2018) studied the acoustic emission (AE) behavior of granite under LN_2 cyclic cooling. They observed that the cooling process increased microcrack density, leading to reduced granite strength.

LN_2 cooling significantly enhances pore structure connectivity, accelerates thermal crack development, and reduces the mechanical strength of rocks. Ultrasonic testing is a non-destructive method commonly used to characterize rock damage. The principle behind this technique is that as ultrasonic waves propagate through the pores and fractures within the rock, attenuation occurs, which reflects the degree of damage (Sun et al., 2022; Al-Ameri and Hamd-Allah, 2023). Fan et al. (2022) measured the P-wave velocity of granite following thermal shock and found a negative correlation between P-wave velocity and both heating temperature and thermal shock. Wanniarachchi et al. (2017) tested the P- and S-wave velocities of various rocks, assessing the mechanical properties of different rock types. While ultrasonic testing provides valuable information regarding rock damage, research in this area remains limited. Most studies on LN_2-induced damage in high-temperature HDR focus on P- and V-wave velocities. Fewer studies examine transmitted waveforms, amplitudes, and dominant frequencies. Therefore, utilizing ultrasonic testing to further explore the damage and fracture characteristics within HDR is crucial for advancing the development of LN_2 fracturing technology.

It is noteworthy that, although numerous studies have investigated the effects of low-temperature LN_2-induced thermal shock on high-temperature reservoir rocks, detailed research on the fracture morphology and failure behavior of reservoir rocks remains lacking. At present, the relationship between the number of LN_2 cooling cycles and fracture connectivity is still unclear, and systematic studies on the underlying damage effects and mechanisms are scarce. It has been confirmed that LN_2 cooling cycles contribute to enhancing the connectivity of reservoir fractures (Yin et al., 2019; Su et al., 2022). As an important indicator for evaluating the artificial fracturing of thermal reservoirs, the fracture behavior and fracture morphology of HDR are closely related to the productivity efficiency of geothermal reservoirs. Therefore, it is essential to investigate the impact of LN_2 cooling cycles on fracture enhancement within geothermal reservoirs.

To explore the fracture morphology and failure behavior of rocks under cyclic heating and LN_2 cooling conditions, this study quantitatively assesses the promoting effect of LN_2 cooling cycles on crack propagation and the changes in fracture surface roughness. The study employs ultrasonic testing technology to comprehensively analyze the damage response of granite during the LN_2 cooling process from multiple perspectives, including wave velocity, waveform, amplitude, and frequency. Through uniaxial compression tests and AE monitoring, the extension of microcracks and fracture behavior of granite under different LN_2 cycle counts are analyzed. Finally, using microscopy, 3D profilometry, and SEM, the internal structural damage and three-dimensional fracture morphology at different LN_2 cycle counts are observed and compared. These findings further reveal the significant role of LN_2 cooling cycles in reducing the cracking pressure of granite and enhancing fracture connectivity. The

results are of great significance for evaluating the frackability of reservoir rocks under various LN_2 cycle conditions.

2. Materials preparation and methods

2.1. Preparation of samples

Granite samples for the experiments were collected from Xuzhou, Jiangsu Province, China (Fig. 1). The samples are light gray and classified as coarse-grained granite. All samples were extracted from the same rock specimen. They were shaped into standard cylindrical specimens measuring 100 mm in height and 50 mm in diameter. The preparation followed the standards set by the International Society for Rock Mechanics and Rock Engineering (ISRM). To control the impact of heterogeneity on the experimental outcomes, rock samples with similar mass and wave velocity were selected for testing.

2.2. Experimental equipment and testing procedures

The study subjected granite samples to repeated cycles of high-temperature heating followed by rapid cooling with LN_2. Subsequent analyses included structural damage characterization, uniaxial compression testing, and fracture morphology examination. The experimental setup and testing procedure are shown in Fig. 2.

Initially, the granite samples were heated in an oven to a target temperature of 300 °C, with a controlled temperature increase of 5 °C/min. To ensure uniform internal and external heating, the samples were maintained at 300 °C for 3 h. After reaching the desired temperature, the samples were promptly transferred to an LN_2 tank (−196 °C) for rapid cooling, where they were held for 1 h. Each heating and LN_2-cooling sequence constituted one complete cycle. The experimental design incorporated eight different cycle counts: 0 cycle, 1 cycle, 3 cycles, 5 cycles, 7 cycles, 9 cycles, 15 cycles, and 20 cycles, to systematically evaluate the effects of repeated thermal stress on the granite samples.

After heat treatment, the granite samples were assessed for structural damage. Ultrasonic testing was used to evaluate the extent of internal damage within the rock (Sang et al., 2020). Specifically, an NM-4A non-metallic ultrasonic flaw detector was employed to examine the internal structure, while surface structural changes were observed using a high-resolution microscope with a resolution of up to 1.1 μm. The source parameters for the ultrasonic system include a sampling period of 0.4 μs, an emission voltage of 500 V, and a sampling length of 512 samples.

Fig. 1. Granite sample.

Additionally, the mass loss of the granite samples was measured using an electronic balance before and after the cyclic treatment to evaluate material degradation. Uniaxial compression tests were subsequently conducted using the TAWD-2000 system under displacement control, with a loading speed of 0.1 mm/min. This system has a maximum axial load capacity of 2000 kN and a load measurement accuracy of ±1 % of the indicated value. During the compression tests, AE monitoring was carried out using the PCI-2 AE system to track the formation and development of internal cracks. The AE system was configured with a pre-amplifier gain of 40 dB and a fixed threshold of 35 dB.

Upon completion of the uniaxial compression tests, the fractured specimens were collected for detailed fracture morphology analysis. The fracture surfaces were scanned using a VR-5000 series 3D profilometer, which offers resolutions up to 160 × and zoom capabilities ranging from 1 × to 4 × . For this analysis, a magnification of 12 × was utilized to capture detailed images of the fracture surfaces. The scanning procedure included: (1) Position Adjustment: The specimen was placed on a rotating platform and adjusted to ensure the fracture surface remained horizontal. (2) Reference Plane Setup: A reference plane was established, and magnification was adjusted for precise measurements. (3) Autofocus: The autofocus function was activated for clarity before measurements. (4) Result Saving: The results were saved for subsequent analysis of fracture morphology and surface roughness.

3. Test results

3.1. Apparent structural changes and mass loss of granite

Fig. 3 presents the results of microscopic observations of the structural changes on the granite surface after multiple cycles of LN_2 cooling. X-ray diffraction (XRD) analysis and the color contrast of mineral grains effectively identify the different mineral compositions in the granite samples. After multiple heating and LN_2 cooling treatments, the microstructure of the granite remained largely unchanged, with no visible macroscopic cracks observed. However, as the thermal cycles progressed, the white texture between the mineral particles gradually appeared, indicating a reduction in the cementation strength between the grains. This phenomenon is consistent with the findings of Wang et al. (2024). Furthermore, detailed observations by Rong et al. (2021) using a high-definition camera revealed significant structural damage to the granite surface after LN_2 cycling. After 15 cycles, as shown in Fig. 3g and h, the white texture became denser and more profound, indicating that the cycling treatment exacerbated the thermal damage to the granite. The temperature gradient is the primary factor responsible for granite damage. During the quenching of high-temperature granite with LN_2, rapid heat exchange between the LN_2 and the hot granite generates intense thermal shock within the rock (Hou et al., 2021). The repeated cycles significantly degrade the physical and mechanical properties of the granite.

Fig. 4 shows the trend of mass change in granite with different thermal cycles. As the frequency of high-temperature heating and LN_2-cooling cycles rises, the percentage of mass loss of the granite gradually increases, though the rate of mass loss diminishes over time. The main factor contributing to this phenomenon is the dehydration of rock minerals and the detachment of fine mineral particles (Hu et al., 2018). At ambient temperature, granite maintains its natural state, containing a certain amount of free and bound water. As high-temperature heating progresses, moisture gradually evaporates, leading to a decrease in mass. Previous studies have shown that the moisture in rock minerals undergoes different dehydration reactions at various temperature ranges,

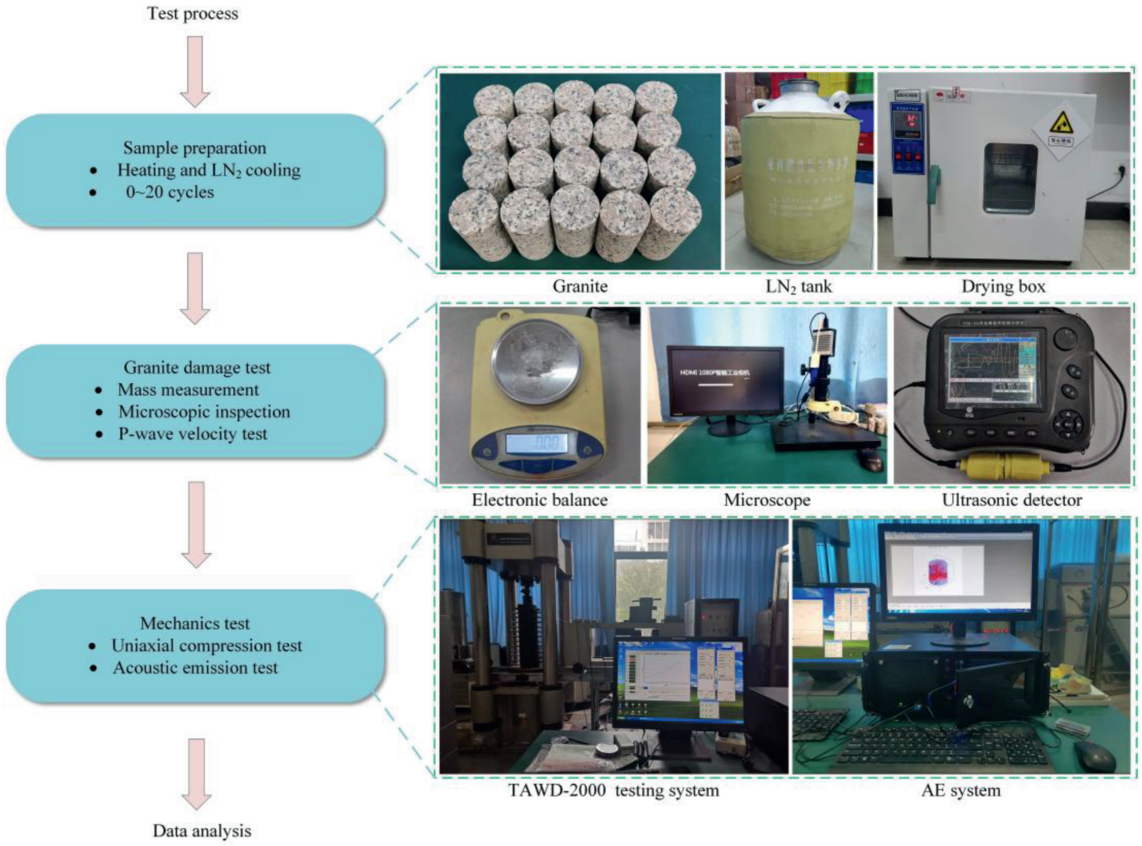

Fig. 2. Experimental procedure diagram.

particularly when the temperature exceeds 100 °C, causing water molecules to escape from the mineral pores (Sun et al., 2015; Zhang et al., 2016). Repeated heating cycles intensify the dehydration of mineral particles, resulting in a continuous reduction in the mass of the granite specimens. After 20 cycles, the sample mass decreased by 0.36 %, showing a small reduction. Following multiple cycles, the mass loss tends to stabilize.

3.2. Evolution of ultrasonic properties of granite at different heating cycle counts

Ultrasonic testing, a widely used non-destructive method in rock mechanics, is employed to evaluate internal damage in rock cores (Li et al., 2023). When ultrasonic waves propagate through fractured rock, they refract at pores and cracks. The superposition of reflected and transmitted waves alters the velocity and waveform of the received signal. By analyzing changes in wave velocity and waveform characteristics, ultrasonic testing effectively reveals the development of pores and cracks within granite samples (Chen et al., 2017).

Fig. 5 presents the ultrasonic time-domain spectra of granite samples subjected to different thermal cycles. To eliminate biases caused by sample density differences and to better capture the changes induced by thermal cycling, this experiment compares the waveform variations (including amplitude and frequency) at different cycle counts with the waveforms of the corresponding intact rock samples. The waveform of the untreated sample is highly regular, characterized by stable amplitude and consistent periods, indicating an intact internal structure in the absence of thermal or mechanical stress. However, as the number of high-temperature heating and LN_2-cooling cycles increases, the regularity and integrity of the waveform gradually deteriorate, accompanied by significant fluctuations in amplitude. Specifically, reductions in the amplitude of the initial wave (3 cycles), central wave (5 cycles, 7 cycles, and 15 cycles), and trailing waves (1 cycle, 5 cycles, and 9 cycles) are observed. These variations suggest that the cumulative thermal damage to the granite intensifies with an increasing number of cycles, progressively compromising the integrity of the internal structure. Notably, after 5 cycles, the waveform becomes severely distorted, with a marked decrease in amplitude. Repeated high-temperature heating and LN_2-cooling induce a greater number and larger area of microcracks within the granite. This extensive microcracking amplifies the diffraction and scattering of sound waves, resulting in significant alterations to both the waveform and amplitude.

By analyzing the changes in the ultrasonic waveform, the degree of damage to the core can be assessed to some extent; however, the frequency characteristics of the signal cannot be directly observed. The frequency reflects the absorption and filtering characteristics of granite towards ultrasonic waves. During the propagation of the waves through the core, the presence of fractures and pores causes attenuation and frequency drift. Thus, transforming the signal from the time domain to the frequency domain makes it easier to analyze signal characteristics like frequency and amplitude. Fourier transform, a widely used computational method, effectively transforms the time-domain ultrasonic signals into their frequency-domain counterparts. The Discrete Fourier Transform (DFT) is represented by the following formula (Sun et al., 2021):

$$X_k = \sum_{n=0}^{N-1} x_n e^{-2\pi i k \frac{n}{N}}, k = 0, 1, \cdots, N-1 \quad (1)$$

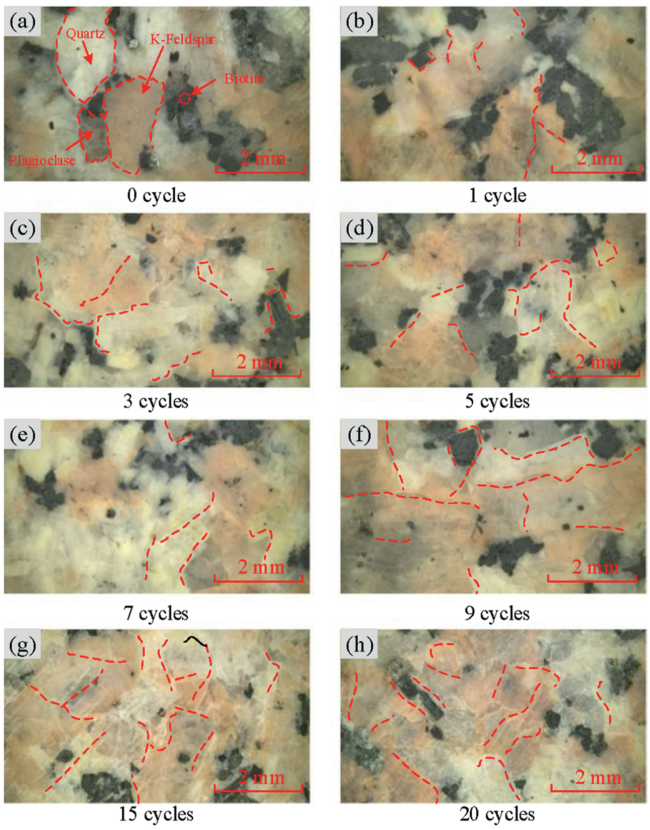

Fig. 3. Surface structure of granite under different thermal cycles.

where X_k is the n-point DFT result for the sequence x_n; $e^{2\pi ik\frac{n}{N}}$ is the N-th complex root of unity; and i is the imaginary unit. Let k be the sampling location, where the sampling location is $0, 1, \cdots, N-1$. The Fast Fourier Transform is a highly efficient algorithm used to compute the DFT, allowing the transition of the ultrasonic signal from the time domain spectrum into the frequency domain spectrum.

In ultrasonic-based internal defect detection of rock materials, the formation of microcracks significantly alters the wave speed, amplitude, and frequency characteristics of the sound waves. Specifically, the propagation speed of ultrasound in the rock medium is directly related to the material's density and elastic modulus. When microcracks form inside the rock, the defect areas experience a local decrease in wave speed due to structural loosening or elastic degradation. Amplitude attenuation reflects the size and shape of the defects. The reflection and scattering effects of microcracks on the sound waves lead to energy dissipation in the transmitted wave, manifested as a significant reduction in amplitude at the receiving end. Frequency response reveals the scale of the defects, with small-scale cracks causing the scattering of ultrasound waves, leading to faster energy attenuation of the high-frequency components. The acoustic response of microcracks exhibits a clear frequency dependence, with changes in the number and scale of microcracks often leading to frequency attenuation and shifts. By comprehensively analyzing the variations in these parameters, both quantitative and qualitative assessments of the microcracks can be achieved.

Fig. 6 presents the ultrasonic frequency spectrum of granite under different thermal cycles. It can be observed that the ultrasonic frequency spectrum mainly consists of a primary frequency peak and several secondary frequency peaks. In the initial state, the primary frequency of granite is approximately 48.92 kHz, with the highest corresponding amplitude intensity, fluctuating between 68.94 dB and 60.74 dB, with an average value of 64.68 dB. The secondary frequencies fluctuate within the range of 0–100 kHz. As the number of high-temperature heating and LN_2-cooling cycles increases, the amplitude of the primary frequency gradually decreases, and the bandwidth increases, while the amplitude and bandwidth of the secondary frequencies decrease accordingly. These changes indicate an increase in the structural damage of the granite. The increase in the primary frequency bandwidth indicates the expansion of large-scale cracks, while the narrowing and eventual convergence of the secondary frequency bandwidth to the primary frequency range suggest that with repeated LN_2-cooling cycles, microcracks gradually connect with the main cracks (Wanniarachchi et al., 2017). Notably, the overall decrease in frequency amplitude indicates the formation of more discontinuous, small-scale microcracks inside the granite. The increased discontinuity and number of thermally induced cracks lead to the differentiation of ultrasonic frequencies, attenuation of the primary frequency peak, and dispersion of energy. Therefore, compared to a single cycle, the more cycles performed, the more pronounced the LN_2 fracturing effect.

Wave velocity and amplitude are among the most intuitive and crucial physical parameters in ultrasonic analysis, as they directly

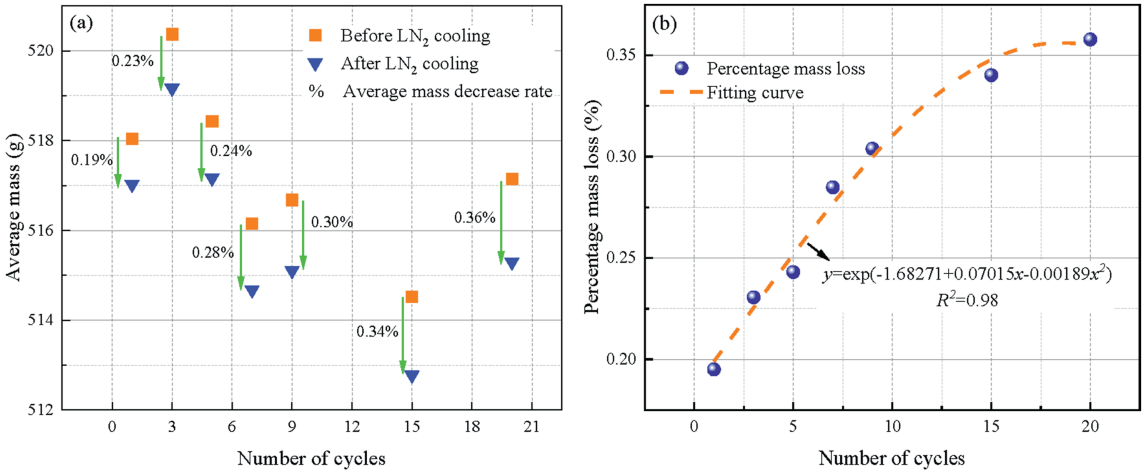

Fig. 4. Variation in granite mass with different thermal cycles: (a) Average mass loss of granite, and (b) Trend of mass loss in granite.

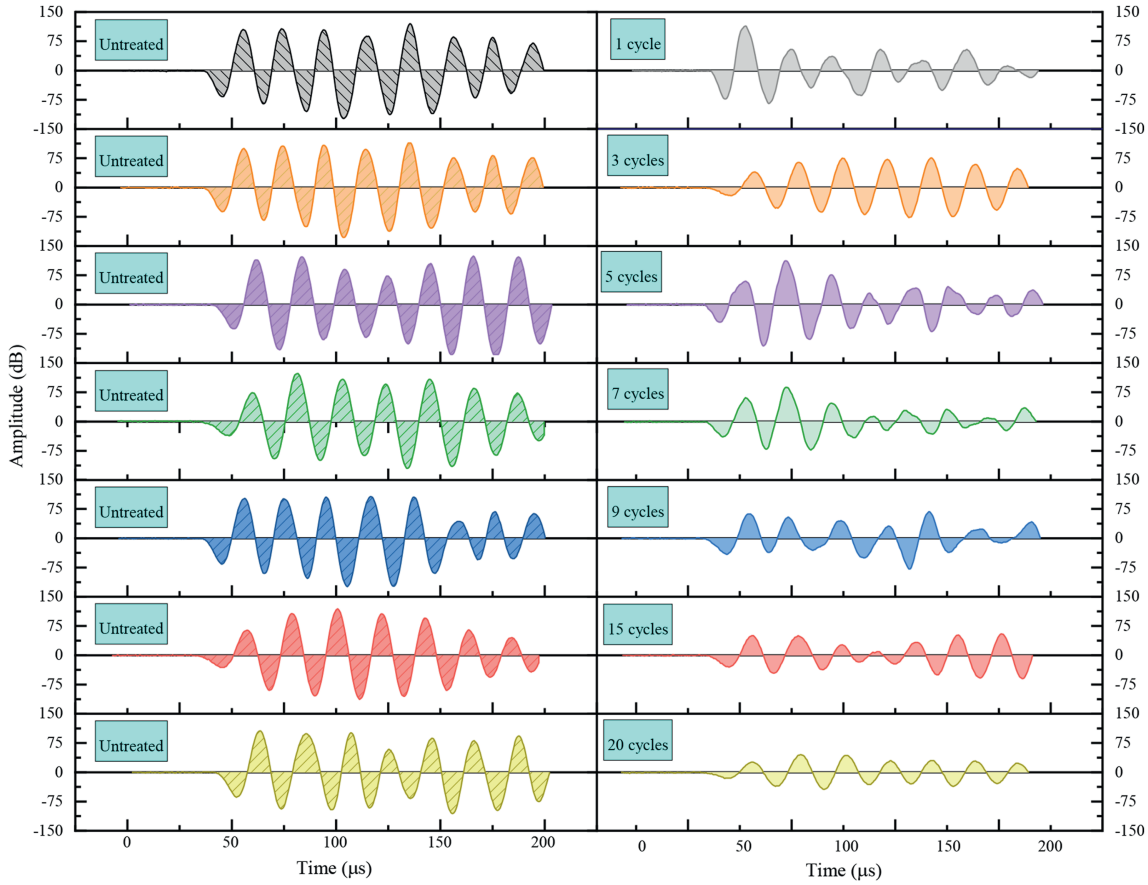

Fig. 5. Ultrasonic time-domain spectra of granite with different thermal cycles.

reflect the amount of structural damage present in the granite. The ultrasonic tests measured the changes in wave velocity and amplitude of each sample before and after the cycles, as shown in Fig. 7. Both P-wave velocity and amplitude exhibit significant reductions with the rise in cycle count. Following a single thermal cycle of heating at high temperature and LN_2-cooling, the P-wave velocity decreased by 39.08 %, representing the maximum reduction observed. During the thermal treatment process, the temperature differential between 300 °C and −196 °C induced thermal cracking in the granite. The formation of thermal fractures compromised the structural integrity of the sample, resulting in ultrasonic energy attenuation as the waves passed through the cracks, thereby reducing the P-wave velocity. With the rise in cycle count, both P-wave velocity and amplitude continued to decrease, although the rate of decline gradually slowed, following an initial rapid decrease, followed by a more gradual reduction. This phenomenon can be attributed to the cyclic stimulation by LN_2, which fully activated the damage potential of the granite. With the rise in cycle count, the propagation of thermally induced cracks slowed down. The cyclic exposure to LN_2 exacerbates this degradation. However, after a certain number of cycles, the P-wave velocity and amplitude reach a stable state, and the internal defects in the granite no longer show significant growth.

3.3. Mechanical property changes in granite with varying thermal cycles

As illustrated in Fig. 8, granite samples exhibit varying stress-strain characteristics after exposure to different thermal cycles. These variations can be attributed to two primary factors: (1) With an increase in the number of cycles, the peak load of the granite decreases gradually, accompanied by a corresponding increase in axial strain. (2) Before reaching the peak, the non-linear deformation characteristics of the stress-strain curve become more pronounced. In the post-peak phase, the continuity of the curve is significantly prolonged, displaying a distinctive “multi-peak” morphology. These findings provide further evidence of the detrimental effects of thermal heating and LN_2-cooling cycles on the internal microstructure of granite, resulting in notable changes to its mechanical properties. The damage to the granite intensifies progressively with an increasing number of cycles, as more pores and microcracks develop. Under external loading, greater axial displacement is required to close these fractures, leading to an extended compaction phase and a pronounced non-linear increase in stress. Additionally, the post-peak phase becomes significantly longer, exhibiting ductile behavior closely associated with the density of thermal cracks in the samples (Ge and Sun, 2018). As axial stress increases, thermal cracks connect with newly formed microcracks, complicating the crack propagation pathways. The cold shock induced by LN_2 cycling not only reduces the fracture initiation stress of the granite but also amplifies the extent of fracturing, thereby enhancing the fracturability of high-temperature granite.

Granite's ability to withstand uniaxial compression and its associated elastic modulus are critical mechanical properties that influence the generation and propagation of cracks during fracturing with LN_2. Fig. 9 illustrates the changes in granite's compressive strength and elasticity with different thermal cycles. Both uniaxial compressive strength and elastic modulus exhibit a nonlinear reduction with the increasing repetition of high-

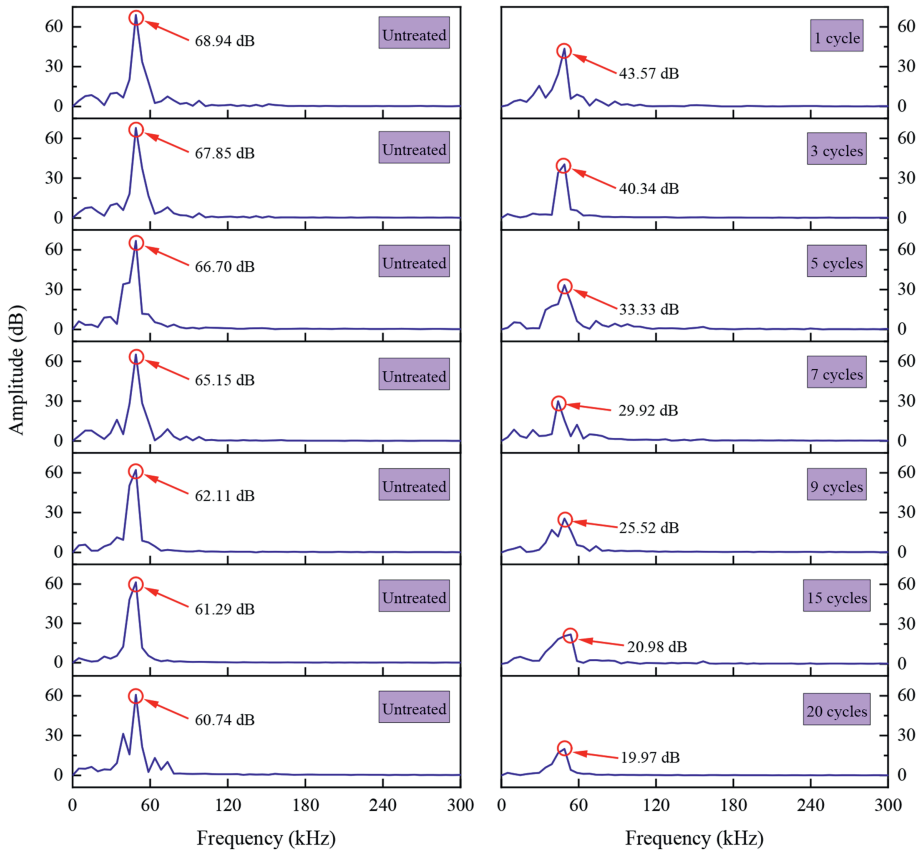

Fig. 6. Frequency domain characteristics of granite with different thermal cycles.

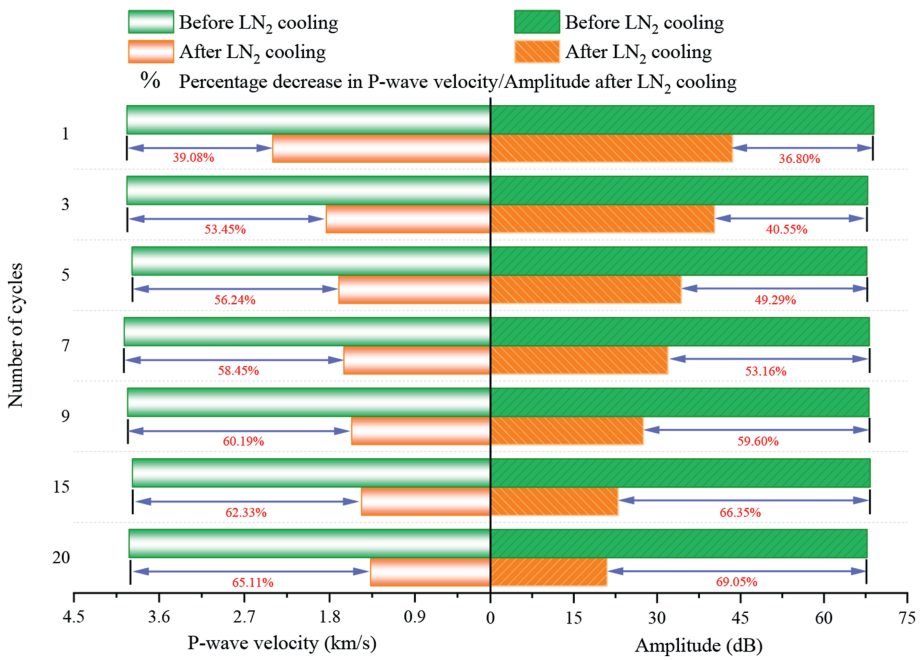

Fig. 7. P-wave velocity and amplitude of granite change with different thermal cycles.

temperature heating and LN_2-cooling cycles. This reduction is primarily attributed to the stimulating effects of LN_2 cycling on the granite's framework structure. Due to thermal stresses, the granite accumulates progressive damage, leading to an increase in internal porosity. This rise in porosity weakens the granite's resistance to deformation and failure, thereby reducing its effective load-bearing capacity. In the first three cycles, the uniaxial compressive strength and elastic modulus showed significant reductions of

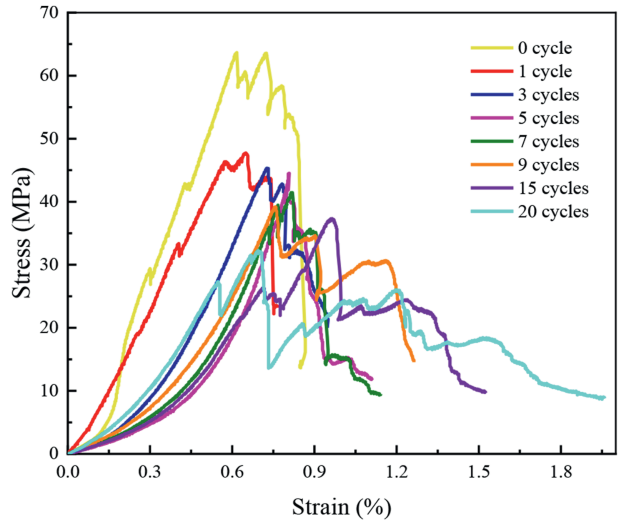

Fig. 8. Stress-strain behavior of granite under different thermal cycles.

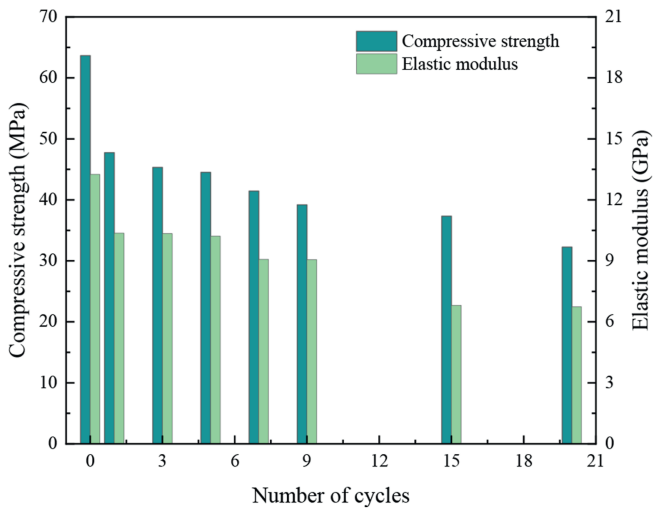

Fig. 9. Variation trends of compressive strength and elastic modulus under different thermal cycles.

28.89 % and 21.96 %, respectively. Over the subsequent 17 cycles, these two parameters decreased further by 20.4 % and 27.17 %, respectively. This indicates that the mechanical properties of granite degrade most significantly during the initial cycles. As the cycle count increases, the deteriorative effects caused by LN_2 thermal shocks become progressively less pronounced. This trend aligns with the changes observed in wave velocity and amplitude.

3.4. Energy evolution during fracture propagation

The deformation and failure of granite are fundamentally energy-driven processes. Throughout the fracture and failure mechanism, these processes are typically accompanied by the absorption, accumulation, dissipation, and release of energy (Chen et al., 2019). The energy imparted to the system reflects the energy required to fracture granite. Therefore, analyzing the evolution of energy during fracture is crucial for elucidating the damage and fracture mechanisms induced by LN_2. This analysis is essential for enhancing rock-breaking efficiency in practical engineering applications and improving the exploitation efficiency of HDR resources.

Under external loading, the structure of granite undergoes damage, with stress at defect sites experiencing sudden changes, leading to the localized release of stress. Therefore, analyzing the damage and fracture characteristics of granite from an energy perspective provides a clearer and more accurate representation of its fracturing behavior. According to the first law of thermodynamics, the strain energy of rocks in uniaxial compression tests can be classified into two categories: A type of strain energy is the elastic deformation energy that can be stored in the rock and recovered reversibly, whereas another form includes the energy associated with surface damage and the plastic deformation required for crack growth, which are irreversible. Based on the definitions of energy input density and elastic energy density, the energy calculation formula is given by

$$U = \int_0^{\varepsilon_i} \sigma_i \mathrm{d}\varepsilon_i \tag{2}$$

$$U_\mathrm{e} = \int_0^{\varepsilon_i^\mathrm{e}} \sigma_i \mathrm{d}\varepsilon_i^\mathrm{e} \tag{3}$$

$$U_\mathrm{d} = U - U_\mathrm{e} \tag{4}$$

where U represents the total energy, U_e denotes the elastic potential energy, U_d refers to the dissipative energy, $\sigma_i (i = 1, 2, 3)$ represents the different principal stresses, $\varepsilon_i (i = 1, 2, 3)$ corresponds to the different principal strains, and $\varepsilon_i^\mathrm{e} (i = 1, 2, 3)$ signifies the different elastic principal strains.

Fig. 10 illustrates a schematic representation of the energy components during rock failure. In this figure, E denotes the elastic modulus in the elastic region of the stress-strain curve under applied load, E_u represents the elastic modulus during unloading, ε^p corresponds to the plastic strain, and ε^e refers to the elastic strain. Taking the peak stress, σ_p, as an example, the area enclosed by *OPB* represents the total energy U^p absorbed by the rock at the peak stress point; the area enclosed by *OAP* corresponds to the dissipative energy U_d^p at the peak stress; and the area enclosed by *ABP* represents the elastic potential energy U_e^p at the peak stress.

The total energy U absorbed by the rock during loading can be calculated by integrating the area under the stress-strain curve

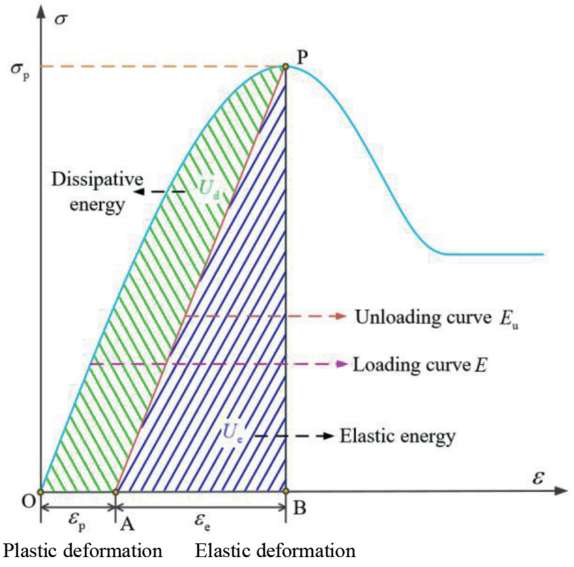

Fig. 10. Schematic diagram of the energy components during rock failure.

and above the coordinate axes, as given by Eq. (2). Simultaneously, the accumulated elastic potential energy U_e of the rock can be computed by determining the area of the triangle *OAP*. Therefore, Eq. (3) can be further transformed into Eq. (5). The specific expression for calculating the elastic potential energy U_e of the rock is as follows:

$$U_e = \int_0^{\varepsilon_i^e} \sigma_i \mathrm{d}\varepsilon_i^e = \frac{1}{2}\sigma\varepsilon_e = \frac{1}{2E_u}\sigma^2 \tag{5}$$

where the elastic modulus E_u of the unloading curve during the rock calculation process can be approximately substituted by the elastic modulus E of the loading curve.

The energy curves for granite, subjected to various heating and LN_2-cooling cycles, are illustrated in Fig. 11. As observed from the figure, during the initial compaction and elastic phases, the total energy absorption curve of granite exhibits a concave upward and nonlinear evolution, which parallels the elastic energy curve. During this phase, a portion of the absorbed energy is used to compact the initial pores and fissures in the granite, while the rest is transformed into elastic energy stored in the rock specimen. The total energy curve increases alongside the elastic strain energy curve, indicating that the granite is undergoing energy accumulation and energy hardening. As the cracks within the granite propagate, the material enters the nonlinear evolution phase, during which the rate of increase in dissipated energy accelerates. The total energy curve starts to deviate from the elastic energy curve. In this stage, most of the absorbed energy is primarily involved in the formation, growth, and merging of new cracks within the material. As the stress in the granite nears its peak, the accumulated elastic energy slowly approaches its maximum storage capacity. Once the peak is reached, accompanied by macroscopic fracture of the granite, the stress rapidly decreases, while the elastic energy curve follows the same evolution trend as the stress-strain curve. At this point, the accumulated elastic energy is released instantaneously, leading to a rapid increase in dissipated energy. Although granite continues to absorb energy during this phase, the absorbed energy is primarily dissipated in the form of dissipative energy.

An analysis of the energy evolution curves for granite exposed to varying heating and LN_2-cooling cycle counts reveals that as the number of cycles increases, the upward concave features of both the total energy curve and the elastic energy curve become more pronounced. This suggests a rise in the initial damage to the granite and a prolongation of the compaction phase. Due to the simultaneous impact of high-temperature heating and LN_2-cooling, the cyclic thermal stresses cause further development of the initial microscopic damage within the rock (such as pores and cracks), and lead to the formation of numerous new microstructural damages. Additionally, starting from the third cycle, both the stress and elastic energy curves of the granite exhibit a characteristic multi-stage drop after the peak. This behavior results from the continuous release of accumulated energy, which induces fractures within the rock. Each fracture causes fluctuations in the elastic energy peak and leads to the establishment of a new stress equilibrium. When the accumulated energy reaches the structural limit, the granite undergoes final fracture. These phenomena indicate that LN_2-cooling induces irreversible damage to granite, increasing the number of initial cracks. As the loading process progresses, the tips of these microcracks further propagate, forming wing cracks that eventually coalesce into weakened regions. This significantly reduces the granite's load-bearing capacity and intensifies its fracture severity.

Fig. 12 depicts the energy evolution patterns at the peak points of granite subjected to various heating and LN_2-cooling cycles. With the rise in cycle count, both the total energy density and elastic energy density show a decreasing trend. This indicates that after multiple cycles, the energy accumulated in the granite diminishes gradually, leading to a significant reduction in its resistance to deformation and failure. In addition to the thermal cracking induced during the heating process, the extreme temperature gradient during LN_2-cooling further damages the granite, leading to a marked alteration in its fracture behavior. Notably, the reduction in elastic energy density is most significant between one and three cycles, reaching 27.6 %. Similarly, the greatest decrease in total energy density occurs between the untreated (0 cycle) and one-cycle samples, amounting to 28.76 %. This suggests that during the first three heating-LN_2-cooling cycles, the physical and mechanical properties of granite experience a notable deterioration. However, with an increasing number of cycles, the damage to the granite does not continue to rise indefinitely; rather, it stabilizes and evolves more slowly.

3.5. Changes in fracture modes

When materials deform and fail due to internal defects under external energy, the resulting elastic waves are referred to as AE. As a non-destructive testing technique, AE plays a crucial role in monitoring rock fracture behavior during mechanical testing (Mansurov, 1994). The macroscopic failure of granite typically originates from the formation of microcracks. By analyzing the AE signals produced during the fracturing and failure of granite, the scale and patterns of these microcracks can be determined.

Fig. 13 shows the physical meaning of the AE characteristic parameters. Cracks in materials are typically categorized into two main types: shear cracks and tensile cracks. By analyzing the rise angle (RA) and average frequency (AF) of the AE parameters, the cracking mechanisms of rocks during the instability and failure process can be identified. Typically, it is understood that tensile crack propagation leads to the generation of longitudinal waves with reduced RA values and increased AF values, whereas shear crack propagation results in shear waves with increased RA values and decreased AF values (Zheng et al., 2023).

Fig. 14 shows the AE event counts and cumulative counts of granite under different thermal cycles. After various cycles of high-temperature heating and LN_2 cooling, significant changes occur in both the mechanical and AE characteristics of the granite. For the untreated samples and the one-cycle samples, the AE activity is more prominent during the pre-peak stage, with the cumulative AE counts showing a stepped increase. Each sudden spike in the cumulative AE counts corresponds to a fluctuation in the stress curve. After three cycles, the AE activity of granite primarily concentrates on the post-peak stage. Not only does the AE event count increase, but their duration also extends. The cumulative AE counts experience significant growth mainly during the post-peak stage, especially after 5 cycles, 9 cycles, and 20 cycles. These differentiated phenomena indicate that the number of cycles significantly influences the internal structure and mechanical properties of the granite. At low cycle numbers (0 cycle and 1 cycle), the damage within the granite is minimal, and the rock exhibits brittle characteristics. Brittle failure is more likely to occur during the pre-peak stage, corresponding to sudden fluctuations in the stress curve and spikes in AE counts. In the post-peak stage, a single main crack often forms, leading to rapid failure. As the number of LN_2 cooling cycles increases, the initial microcracks in the granite increase, and the compaction phase is extended (shown by a smooth, concave stress curve), thereby enhancing the toughness of the granite. During the post-peak stage, microcracks interconnect and form macroscopic cracks, resulting in stress release and structural failure, ultimately leading to multi-stage

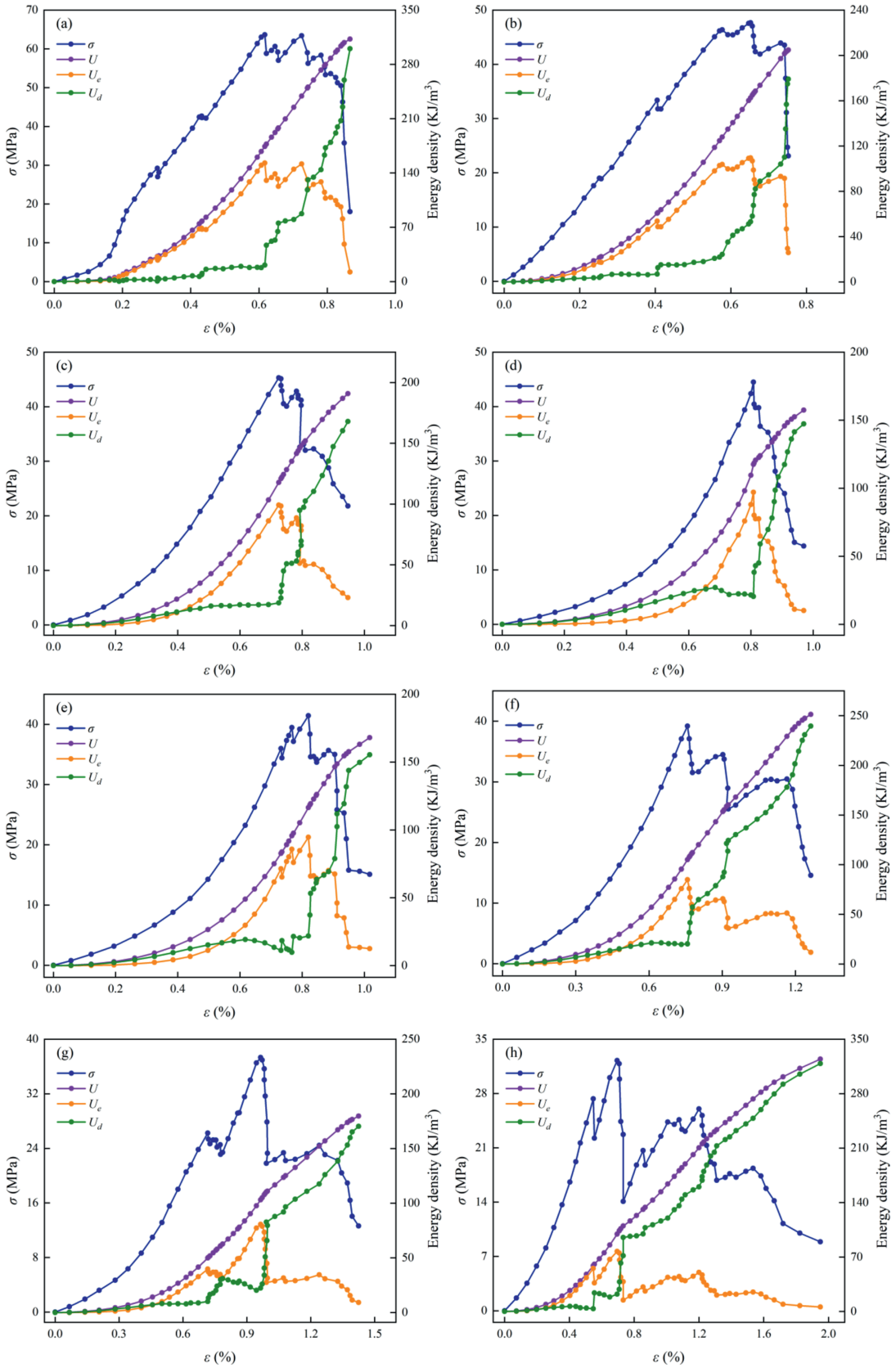

Fig. 11. Energy evolution curves of granite at different thermal cycles: (a) 0 cycle; (b) 1 cycle; (c) 3 cycles; (d) 5 cycles; (e) 7 cycles; (f) 9 cycles; (g) 15 cycles; and (h) 20 cycles.

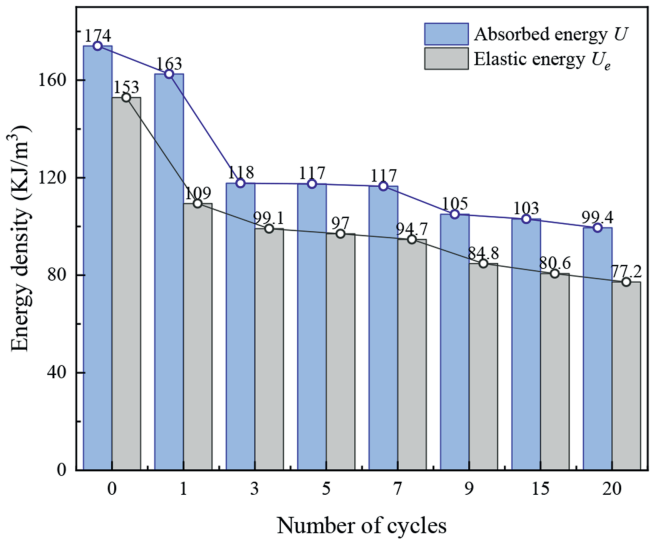

Fig. 12. Energy evolution patterns at peak points of granite under different thermal cycles.

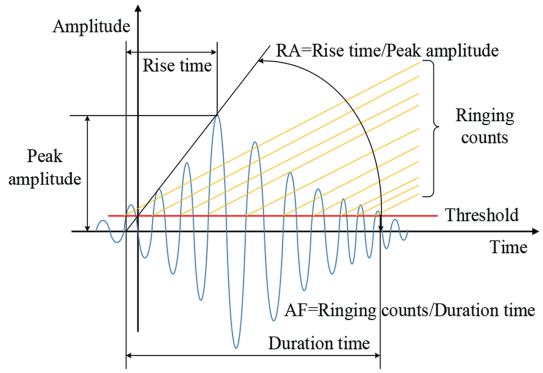

Fig. 13. Graphical representation of AE characteristic parameters.

fractures. At this point, AE activity becomes frequent, and the cumulative counts increase rapidly. The results of the study show that after multiple LN_2 cooling cycles, not only is the crack initiation pressure of the granite reduced, but the formation of a complex fracture network is also facilitated.

Fig. 15 illustrates granite's AF-RA data distribution with different thermal cycles, with the blue region representing the high-density area of AE data. The variation in the high-density region with respect to cycle number reflects the growth and pattern of microcrack propagation in the granite. It can be observed that with an increasing number of high-temperature heating and LN_2-cooling cycles, the high-density region gradually changes from an initial "I" shape to a "b" shape. A large temperature contrast between high-temperature heating and LN_2-cooling results in the formation of thermal gradients within the granite, causing mineral particles to undergo compressive deformation due to uneven heating, which subsequently leads to thermal cracking. Under loading, the extent and propagation rate of microcracks increase with the presence of larger initial defects. Notably, in addition to the increase in the number of AE signals, the characteristics of these signals shift from "high AF - low RA" to "high RA - low AF". This indicates that granite with more severe thermal damage exhibits a greater number of shear microcracks under loading, which is associated with the initial damage density induced by thermal stress. As more high-temperature heating and LN_2-cooling cycles are applied, the initial damage grows markedly. Under axial stress, the damaged regions are more prone to unstable crack propagation, resulting in a higher occurrence of shear microcracks.

Furthermore, the crack patterns during the fracture process of granite can be quantified based on the specific ratio between AF and RA. According to previous studies (Du et al., 2020), in this study, the equation $AF = 110RA + 60$ defines the boundary between tensile and shear cracks. As shown in Fig. 16, the ratio of tensile cracks to shear cracks in granite specimens changes with the number of heating and LN_2-cooling cycles. In the cycle range from 0 to 20, the percentages of tensile cracks are as follows: 55.9 %, 52.1 %, 34.7 %, 29.7 %, 28.1 %, 26 %, 25 %, and 16.1 %, respectively. The results indicate that, starting from the third cycle, there are more tensile cracks than shear cracks, suggesting a shift in the fracture mode of granite. At low cycle numbers (0 and 1), the damage caused by LN_2 cold shock is limited, and the induced microcracks primarily propagate along the internal matrix surfaces, with intergranular cracks being predominant. This leads to tensile fracture as the primary failure mode in granite. At high cycle numbers (3–20), the cumulative damage caused by LN_2 cold cycling results in a considerable decrease in the strength of mineral grains and their bonding forces. This leads to the simultaneous development of transgranular and intergranular cracks, which shifts the dominant fracture mode of granite to shear failure (Wang et al., 2016).

Furthermore, the increase in the proportion of shear cracks corroborates the evolution of the AE event count. The LN_2 cooling cycle induces the formation of more micro-cracks inside the granite. Under external loading, these micro-cracks connect, creating weak planes within the granite. As the load continues to increase, these weak planes are the first to fail, leading to a drop in stress and a surge in AE events. At this point, the granite has not fully failed; internal stress within the granite is redistributed (e.g. through granular crushing, frictional sliding), and it still retains some compressive strength. As external loading continues, the granite undergoes multi-stage fractures, ultimately leading to failure. Throughout this process, the AE event count remains highly active, and the increase in the proportion of shear cracks also indicates that the fracture mode becomes more complex.

Figs. 17–19 show the AF-RA data distribution of granite at different stages under 3 cycles, 5 cycles, and 9 cycles, respectively. Based on the total stress curve of granite, its failure process can be divided into five stages: I: Compaction stage, II: Elastic stage, III: Crack stable propagation stage, IV: Crack unstable propagation stage, and V: Post-peak stage. As shown in Fig. 17a, 18a and 19a, during the compaction and elastic stages (stages I and II), the AF and RA curves remain relatively stable. During these stages, the initial cracks in the granite close, the granite remains in a low-stress state, and fewer microcracks are generated, mostly in the form of tensile cracks. As the loading time increases, the AF and RA curves begin to fluctuate. Overall, AF shows a downward trend, while RA shows an upward trend, with the ratio between the two increasing over time. This indicates that with increasing external load, internal cracks start to initiate and propagate, and the number of shear microcracks increases. Particularly during the crack propagation stages (III and IV) and the post-peak stage (V), the AF and RA curves experience significant fluctuations, with both tensile and shear cracks developing concurrently.

Notably, each drop in the stress curve corresponds to a sharp decrease in the AF curve and a surge in the RA curve. This suggests that the cracks that ultimately lead to granite failure are predominantly shear cracks. By comparing the AF-RA data distribution at different stages, it is also observed that the AE data extends

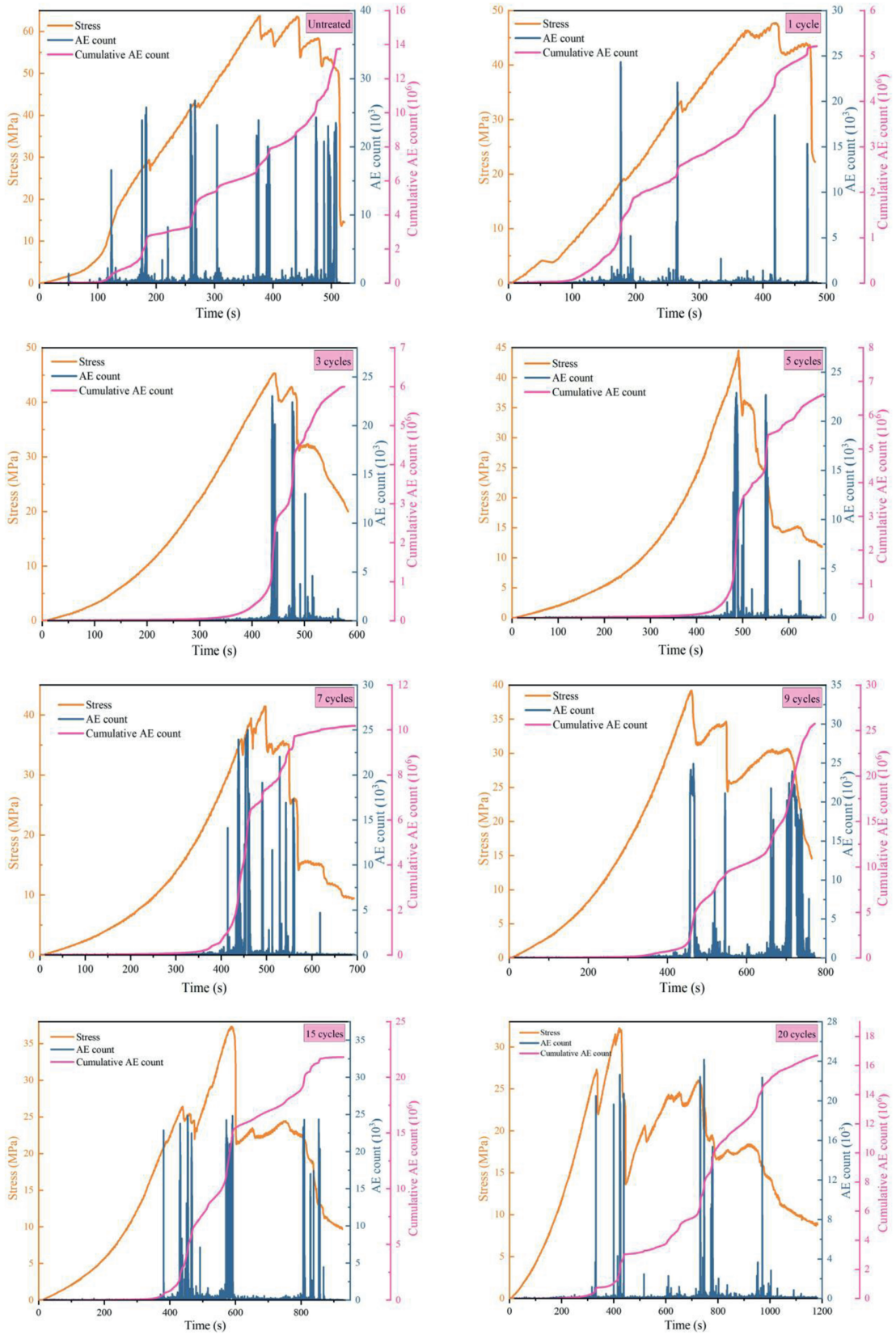

Fig. 14. AE event counts and cumulative counts of granite under different thermal cycles.

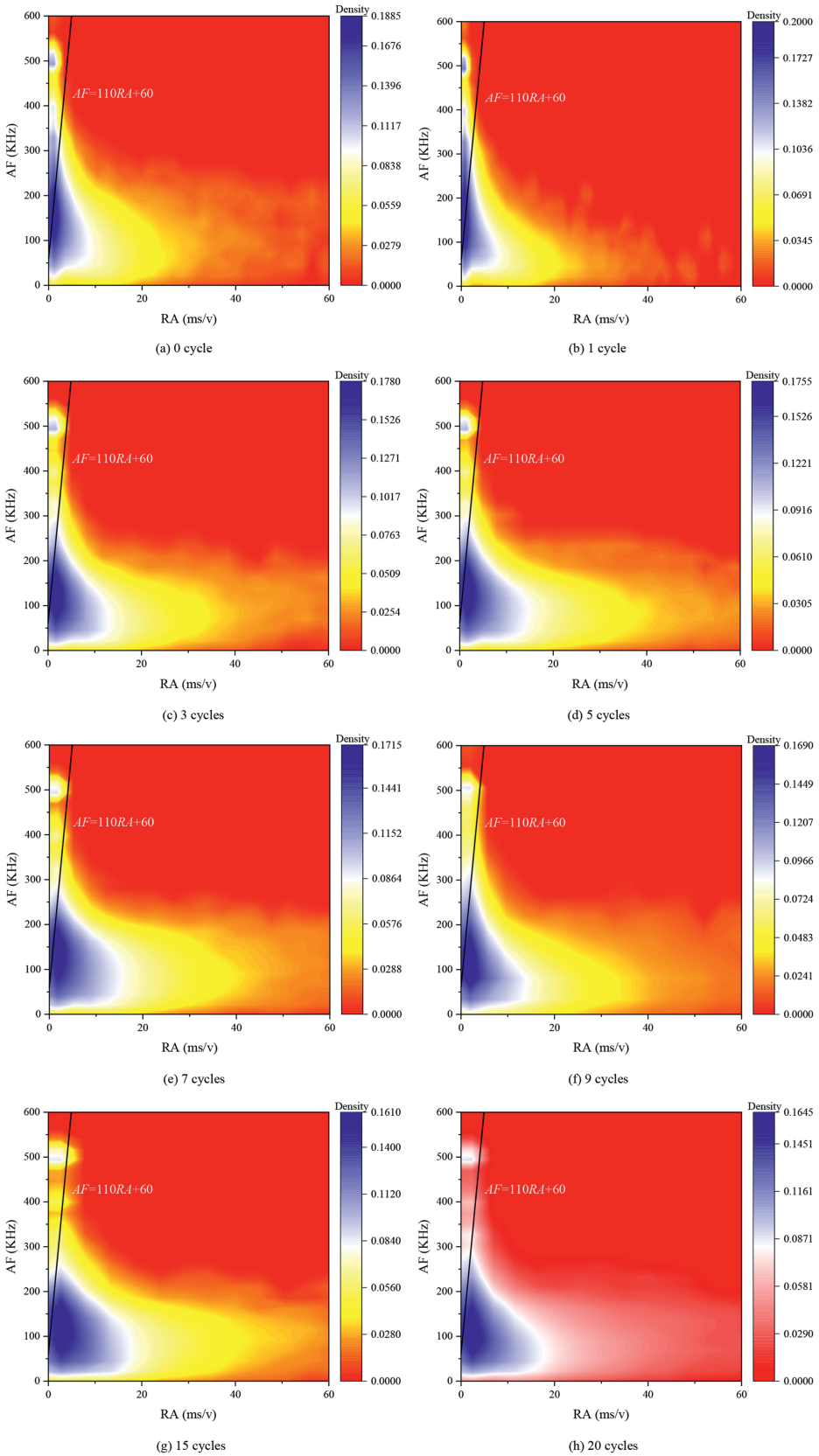

Fig. 15. Distribution of AF-RA data for granite under different thermal cycles.

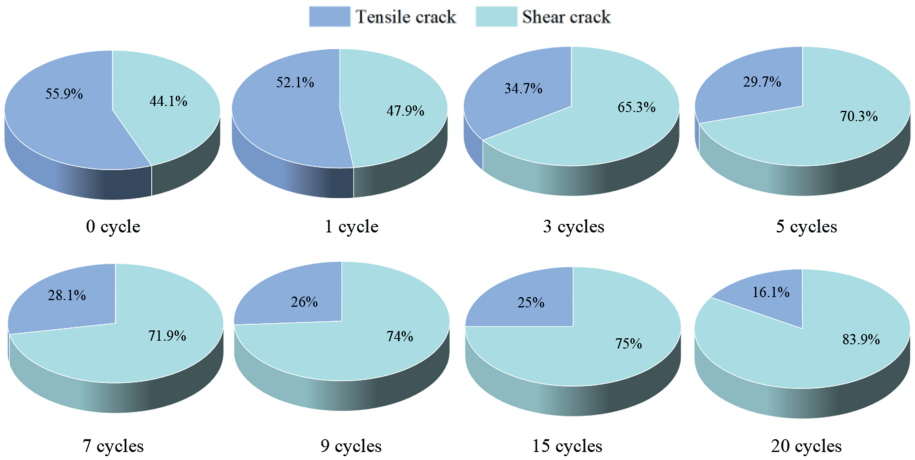

Fig. 16. Ratio of tensile to shear cracks in granite samples under different thermal cycles.

towards the RA axis. This indicates that both shear and tensile cracks increase during the failure process, with shear cracks growing at a higher rate. Additionally, by comparing the AF-RA data distribution for different cycles, it is found that granite subjected to more LN_2-cooling cycles generates a higher proportion of shear cracks during the crack propagation and post-peak stages. The high-temperature heating and LN_2-cooling cycles cause damage to the granite's microstructure (such as crystal defects and microcrack distribution), making the fracture path more complex and more prone to shear failure.

The crack morphology of rocks directly reflects their fracture characteristics and the extent of damage. During the experiment, granite fractures along multiple fracture surfaces. This study selected the primary fracture surface (the one through which the main crack propagates) for morphological measurements, as it has the largest area, most accurately represents the overall fracture behavior, and provides the most reliable data for analyzing surface roughness and fracture mechanisms. Fig. 20 depicts the macroscopic fracture patterns of granite specimens after undergoing different thermal cycles. As shown in Fig. 20a, granite primarily exhibits three fracture modes under uniaxial compression: tensile failure, single-shear plane failure, and X-type conjugate shear failure. Notably, when initial fractures are present within the granite, complex fracture modes, such as Y-type failure and multi-fracture failure, can also occur. As shown in Fig. 20b, after 0 cycle and 1 cycle of processing, the fracture mode of granite is predominantly tensile failure. Under axial compression, the induced lateral tensile stresses exceed the granite's ultimate tensile strength, causing the fracture to propagate along the axial direction, with multiple tensile cracks visible on the surface parallel to the axis. Starting from the third cycle, the primary fracture plane of the granite undergoes a significant transition to an inclined shear crack. This indicates that, from the third cycle onward, the fracture mode of the granite shifts from axial tensile failure to a single shear failure along an inclined plane. This experimental result is consistent with the classification of AF-RA in the AE data. With an increase in the number of high-temperature heating and LN_2-cooling impact cycles, the number, depth, and tortuosity of macroscopic cracks in granite further increase. Both primary and secondary fractures develop concurrently, resulting in a complex fracture morphology. This indicates that the structural damage caused by LN_2 affects the propagation direction of the fracture path. After multiple cycles of treatment, LN_2 induced a larger number of more complex microcracks. The complexity of these microcracks promoted the development of more intricate shear fracture paths within the sample. Under applied loading, these complex microcracks rapidly propagate, ultimately resulting in a shift in the macroscopic fracture morphology of the granite.

3.6. Analysis of fracture morphology and surface roughness

The morphological characteristics of granite fracture surfaces are essential for studying rock deformation and failure. The extent of damage to granite is influenced by the number of heating and LN_2-cooling cycles, and the fracture surfaces formed after rock failure exhibit distinct differences. The morphological features of the fracture surfaces allow for a qualitative analysis of crack propagation and fracture modes, indirectly reflecting the degree of damage to the rock's microstructure.

Fig. 21 presents three-dimensional cross-sectional images of granite fracture surfaces under different thermal cycles. After 0 cycle and 1 cycle, the internal damage to the granite is relatively minor, with fewer microcracks and no significant surface undulations. Starting with the sample subjected to 3 cycles, larger valleys and peaks become evident, and the fracture surface exhibits more pronounced undulations. As the cycle count increases, extensive undulations appear in the diagonal regions of the fracture surface, displaying typical shear failure characteristics. This results from the combined effects of high-temperature heating and LN_2-cooling on the granite. Under these conditions, pre-existing microcracks expand irregularly while new microcracks continue to nucleate. The interaction between the growth of existing and newly formed cracks creates weak zones, progressively reducing the rock's load-bearing capacity.

As axial pressure increases, microcracks gradually connect and propagate, leading to the formation of interconnected weak zones. These weak areas fail first, after which macroscopic failure cracks extend into other weak regions. This process ultimately results in the development of characteristic shear failure features. Moreover, with an increasing number of cycles, the step-like features on the fracture surface become more pronounced. This further indicates that, compared to a single LN_2-cooling cycle, repeated cooling cycles are more likely to induce the formation of large-scale, complex crack networks. The development of these crack networks increases the contact area between the heat exchange medium and the reservoir rock, which is critical for improving the efficiency of geothermal energy extraction.

Roughness and complexity are key attributes for characterizing fracture surface morphology. By selecting appropriate feature parameters based on the measurement of fracture surfaces, the

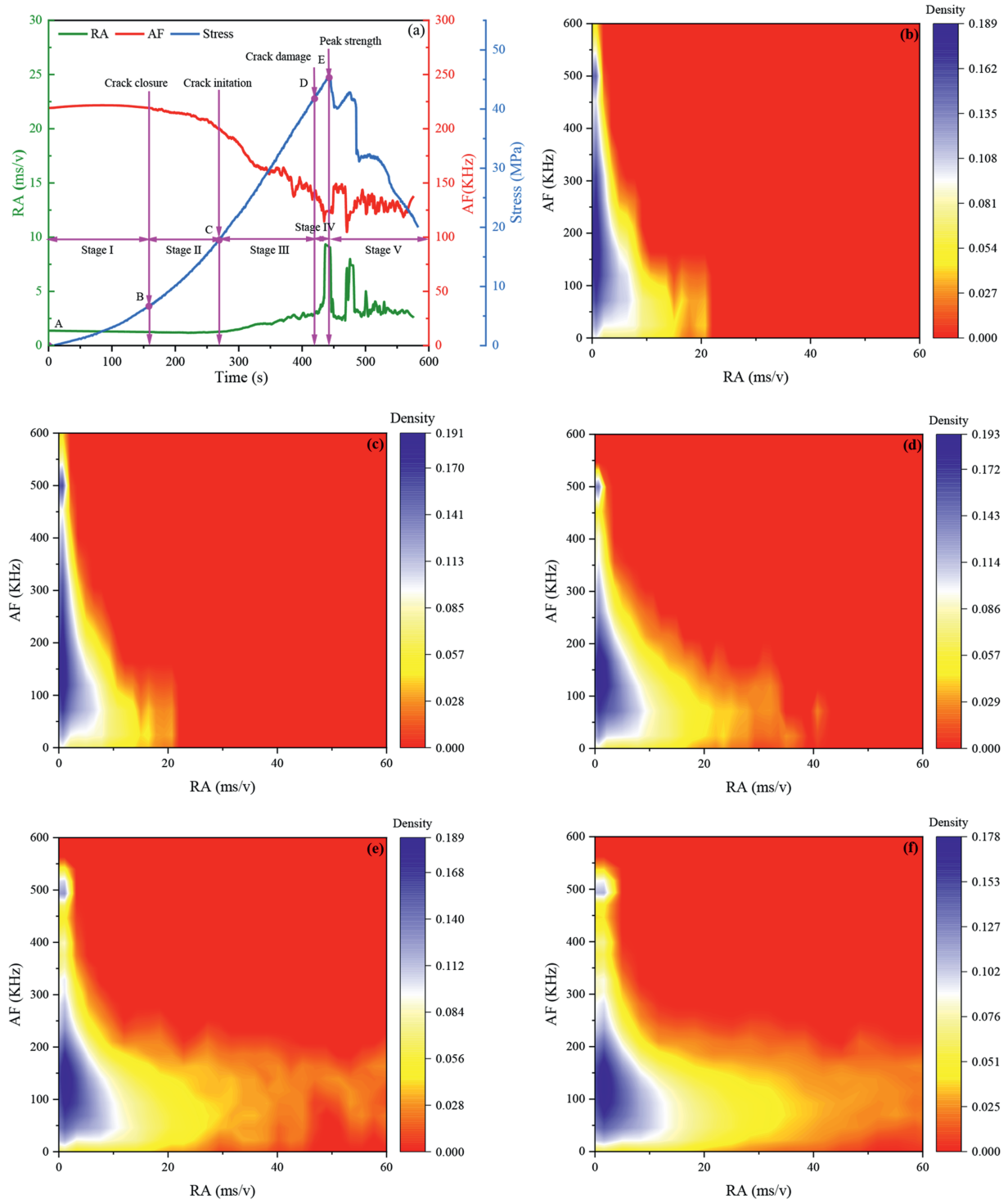

Fig. 17. Distribution of AF-RA data at different stages of granite under 3 cycles: (a) Total stress diagram; (b) Stage I; (c) Stage II; (d) Stage III; (e) Stage IV; and (f) Stage V.

roughness and complexity of rock fracture planes can be effectively quantified. Common feature parameters include: (1) arithmetic mean height S_a, defined as the average vertical distance of all points in the surface area to the reference plane; (2) root mean square height S_q, representing the standard deviation of the vertical distances between the surface points and the reference plane; (3) maximum height S_z, which refers to the total height difference between the highest peak and the lowest valley within the surface area; and (4) fractal dimension D_F, calculated using the box-counting method (Wanniarachchi et al., 2017; Su et al., 2022). The specific calculation formulas for the feature parameters are as follows (Jia et al., 2018):

$$S_a = \frac{1}{A}\iint |z(x,y)|\mathrm{d}x\mathrm{d}y \tag{6}$$

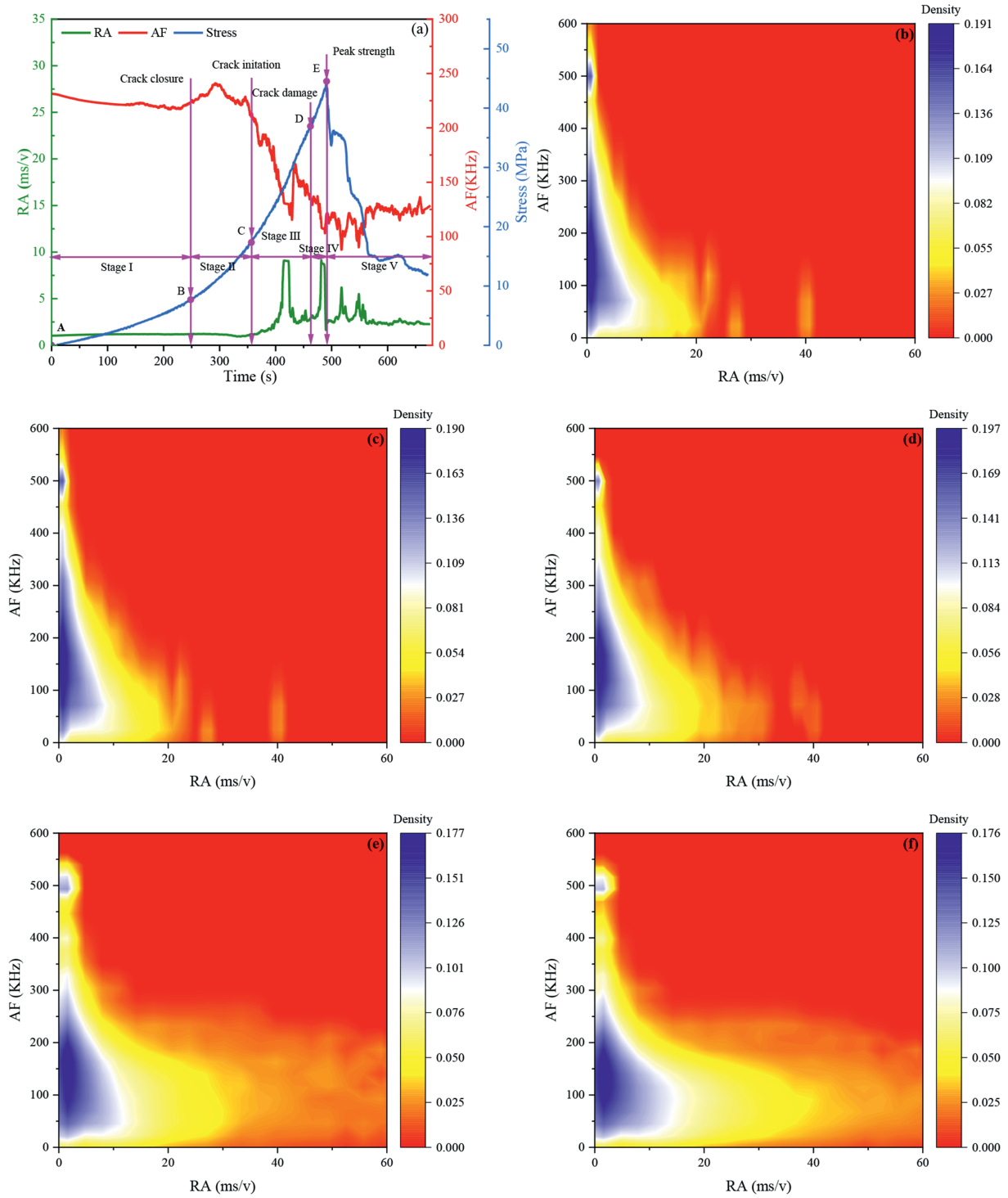

Fig. 18. Distribution of AF-RA data at different stages of granite under 5 cycles: (a) Total stress diagram; (b) Stage I; (c) Stage II; (d) Stage III; (e) Stage IV; and (f) Stage V.

$$S_q = \sqrt{\frac{1}{A}\iint z^2(x,y)\mathrm{d}x\mathrm{d}y} \tag{7}$$

$$S_z = S_p + S_v \tag{8}$$

where A represents the area of the surface region; (x, y) denotes the coordinates (both horizontal and vertical) of the points within the surface area; $z(x, y)$ is the height function corresponding to the coordinates of each point; S_p denotes the maximum peak height; and S_v denotes the maximum valley depth.

Fig. 22 illustrates the evolution of the roughness feature parameters of the granite fracture surface with different thermal cycles. It can be observed that the trends of change for the four feature parameters, arithmetic mean height S_a, root mean square height S_q, maximum height S_z, and fractal dimension D_F are consistent, all of which increase with the number of heating and LN_2-cooling cycles. After 20 cycles, the maximum increases in the

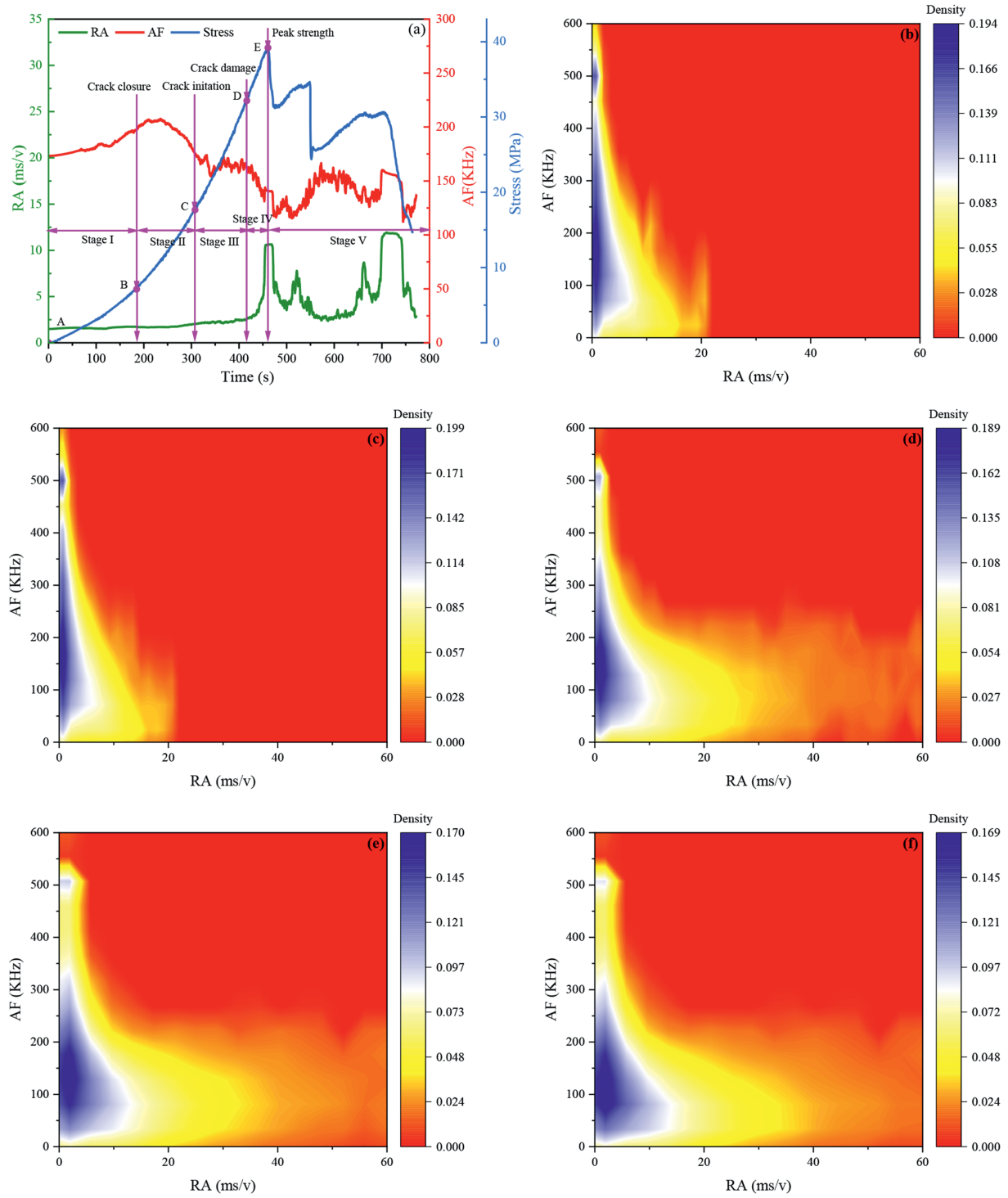

Fig. 19. Distribution of AF-RA data at different stages of granite under 9 cycles: (a) Total stress diagram; (b) Stage I; (c) Stage II; (d) Stage III; (e) Stage IV; and (f) Stage V.

four feature parameters were 277.43 %, 226.16 %, 202.68 %, and 4.03 %, respectively. The increase in these feature parameters indicates that the roughness of the rock fracture surface also increased accordingly. By comparing the four feature parameters, it can be observed that the increases in arithmetic mean height S_a and root mean square height S_q are similar across different cycling iterations, with significant increases occurring at the 3 cycles and 9 cycles. In contrast, the growth rates of maximum height S_z and fractal dimension D_F remain relatively stable across all cycles. After the number of cycles exceeds 9, the growth rate of the four feature parameters S_a, S_z, S_q, and D_F significantly slows down, and the rate of increase becomes notably smaller. The results of the study indicate that when LN_2 is used to assist in fracturing high-temperature granite, the cooling effect of LN_2 makes the fracture surface morphology more complex. However, this complexity and roughness do not increase indefinitely with the number of LN_2 treatments. Therefore, simply increasing the number of LN_2-cooling cycles to enhance geothermal energy production from the

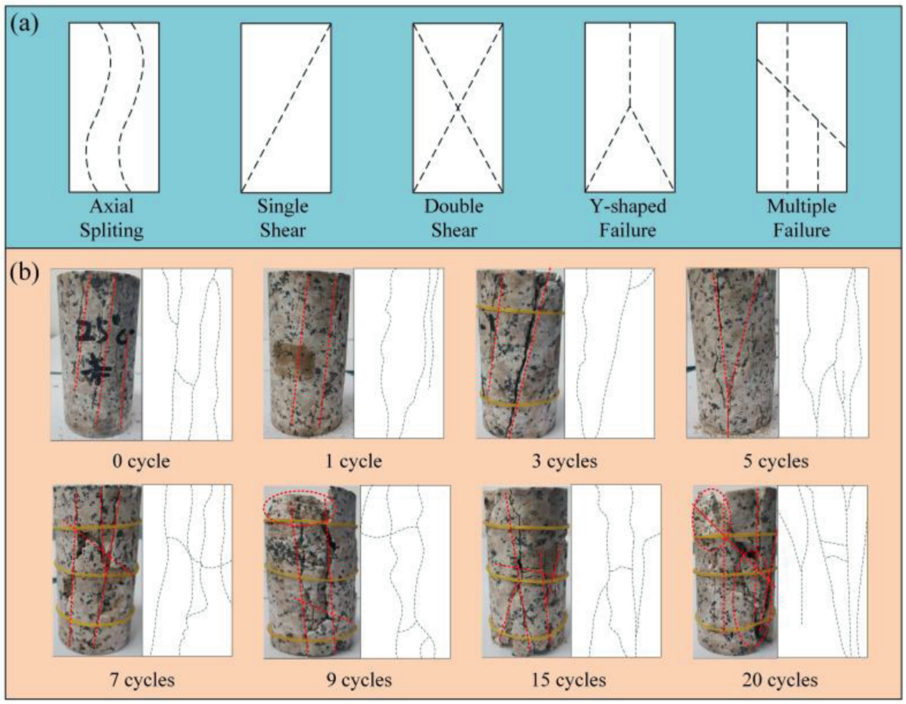

Fig. 20. Macroscopic fracture modes of granite under different thermal cycles. (a) Schematic diagram of fracture; and (b) Photographs of actual fracture.

reservoir is not a feasible approach.

4. Discussion

4.1. The association between P-wave velocity, mechanical behavior, and surface roughness

The research highlights that both physical parameters and mechanical properties effectively reflect the impact of thermal exposure, including high-temperature heating and LN_2-cooling, on granite degradation. Among these, P-wave velocity is particularly sensitive to microstructural damage and serves as a reliable indicator of changes in granite porosity. Key mechanical parameters, such as uniaxial compressive strength and the elastic modulus, reveal significant alterations in the macroscopic mechanical behavior of granite, directly resulting from microstructural changes. Additionally, roughness parameters provide a quantitative measure of the modifications in the fracture surface morphology of granite following thermal treatment and mechanical testing. Building on these findings, the current study explores the relationship between P-wave velocity, mechanical parameters, and surface roughness, aiming to establish a comprehensive understanding of how thermal and mechanical processes influence granite's structural and mechanical integrity.

As shown in Fig. 23, P-wave velocity and mechanical parameters are interrelated. The results indicate a strong linear correlation between granite's P-wave velocity, uniaxial compressive strength, and elastic modulus. With an increase in uniaxial compressive strength and elastic modulus, granite's P-wave velocity also increases, showing a positive correlation. Moreover, numerous studies have shown that changes in the mechanical behavior of granite after thermal exposure can be reliably monitored through P-wave velocity (Sharma and Singh, 2008; Pappalardo, 2015; Lü et al., 2017; Jamshidi et al., 2018).

As shown in Fig. 24, P-wave velocity and roughness parameters are interrelated. The study reveals a nonlinear inverse correlation between P-wave velocity and roughness parameters; as the roughness increases, granite's P-wave velocity decreases. Notably, during the 0 to 3 cycles, P-wave velocity decreases sharply as the roughness parameters increase. However, from 3 cycles to 20 cycles, this decline becomes slower. This phenomenon further highlights that granite's physical and mechanical characteristics are significantly influenced by high-temperature heating and LN_2-cooling cycles. Under low cycle conditions, the pore structure of granite deteriorates notably, as evidenced by an increase in microcrack formation. With a higher number of cycles, the generation of new cracks diminishes, and the connectivity between cracks strengthens. Consequently, under high-cycle conditions, P-wave velocity stabilizes, while roughness continues to increase, which enhances the fracturability of high-temperature reservoir rocks.

4.2. Assessment of thermal shock damage

The repeated high-temperature heating treatment followed by LN_2-cooling caused substantial thermal shock damage to the granite specimens. In fact, the alterations in the granite's physical and mechanical characteristics serve as indicators of the extent of this thermal shock damage. To evaluate the degree of thermal damage in granite, we calculated three damage indicators based on P-wave velocity, uniaxial compressive strength, and elastic modulus. Thermal damage in granite can be defined as

$$D_N = 1 - \frac{I_N}{I_0} \tag{9}$$

where D_N represents the degree of damage to the granite following N cycles of high-temperature heating and LN_2-cooling, while I_0 and I_N correspond to the physical and mechanical characteristics of the granite following 0 and N cycles, respectively. The results of thermal damage analysis based on various mechanical properties are shown in Fig. 25. The damage results, denoted as D_V, D_E, and

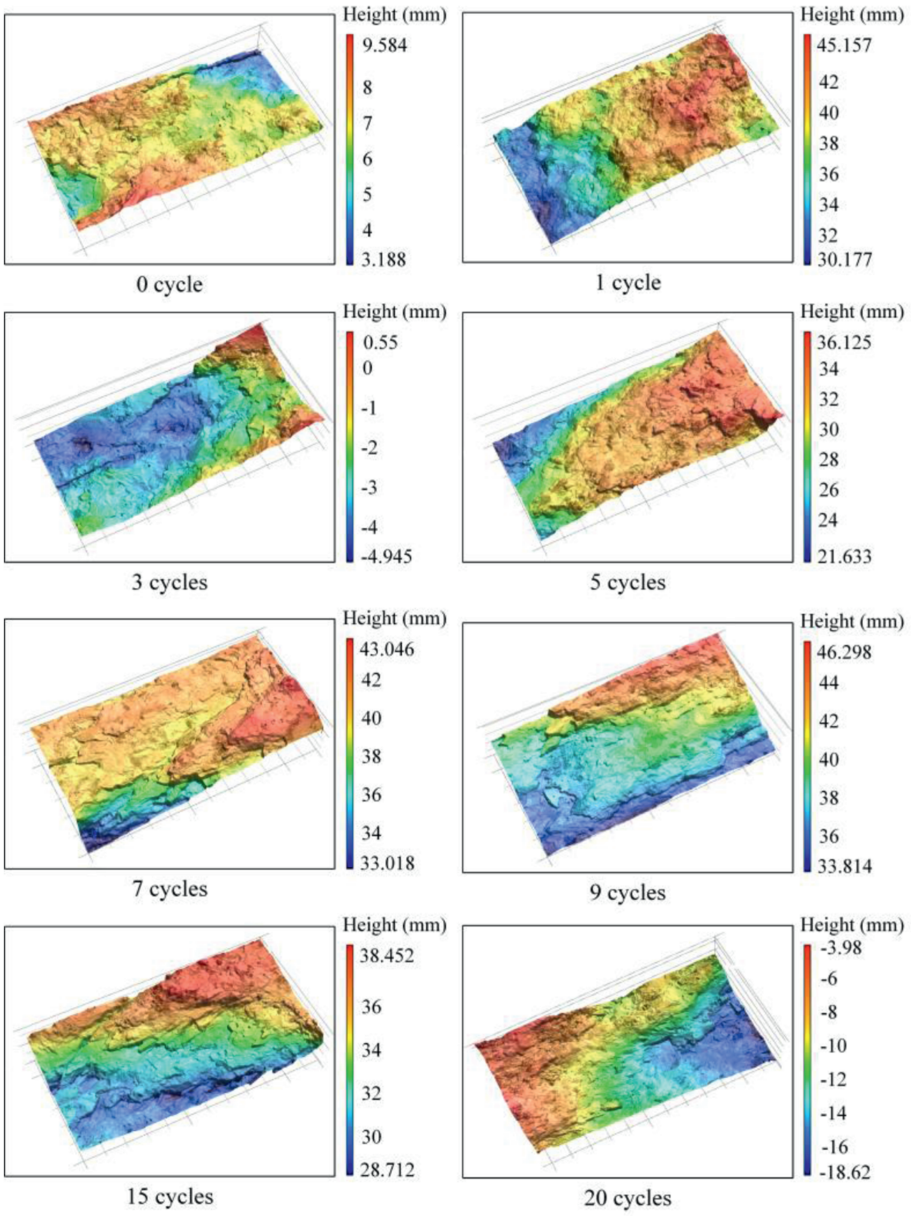

Fig. 21. Three-dimensional cross-sectional images of granite fracture surfaces at different thermal cycles.

D_{UCS}, calculated from P-wave velocity, elastic modulus, and uniaxial compressive strength, respectively, all show the same trend: The extent of granite damage grows based on the count of high-temperature heating and LN_2-cooling cycles. However, the damage values derived from different physical and mechanical parameters vary, with the value based on P-wave velocity being notably higher.

The amount of the energy intake of the granite samples is primarily utilized for crack initiation and propagation. Granite sustains different extents of thermal damage as a result of heating and LN_2-cooling cycles, which subsequently affects the energy required for fracture failure. Consequently, a relationship exists between the energy absorbed by granite under external loading and its thermal damage. Fig. 26 shows the relationship between absorbed energy and thermal damage values under different cycles. The thermal damage values, calculated using various mechanical parameters, exhibit a strong linear correlation with the absorbed energy of granite. As thermal damage increases, the energy required for fracture decreases. Among the parameters, D_V and D_{UCS} show the strongest correlation is with the absorbed energy, $R^2 > 0.8$. After high-temperature heating and LN_2-cooling, the granite matrix exhibits a degradation in its physical and mechanical properties, leading to a decrease in its ability to store elastic energy. Consequently, compared to untreated samples, specimens with higher thermal damage values require less energy to reach the damage threshold. Additionally, the energy required for the propagation of microcracks is significantly lower than that for their initiation (Xi et al., 2023). With more cycles, the number of microcracks grows, causing a further increase in the thermal damage value. Under external loading, microcracks propagate and coalesce with relatively low energy, forming a network of cracks, which ultimately leads to the fracture failure of granite.

Fig. 27 shows the evolution of granite mechanical parameters with different cycle numbers. The study indicates that as the

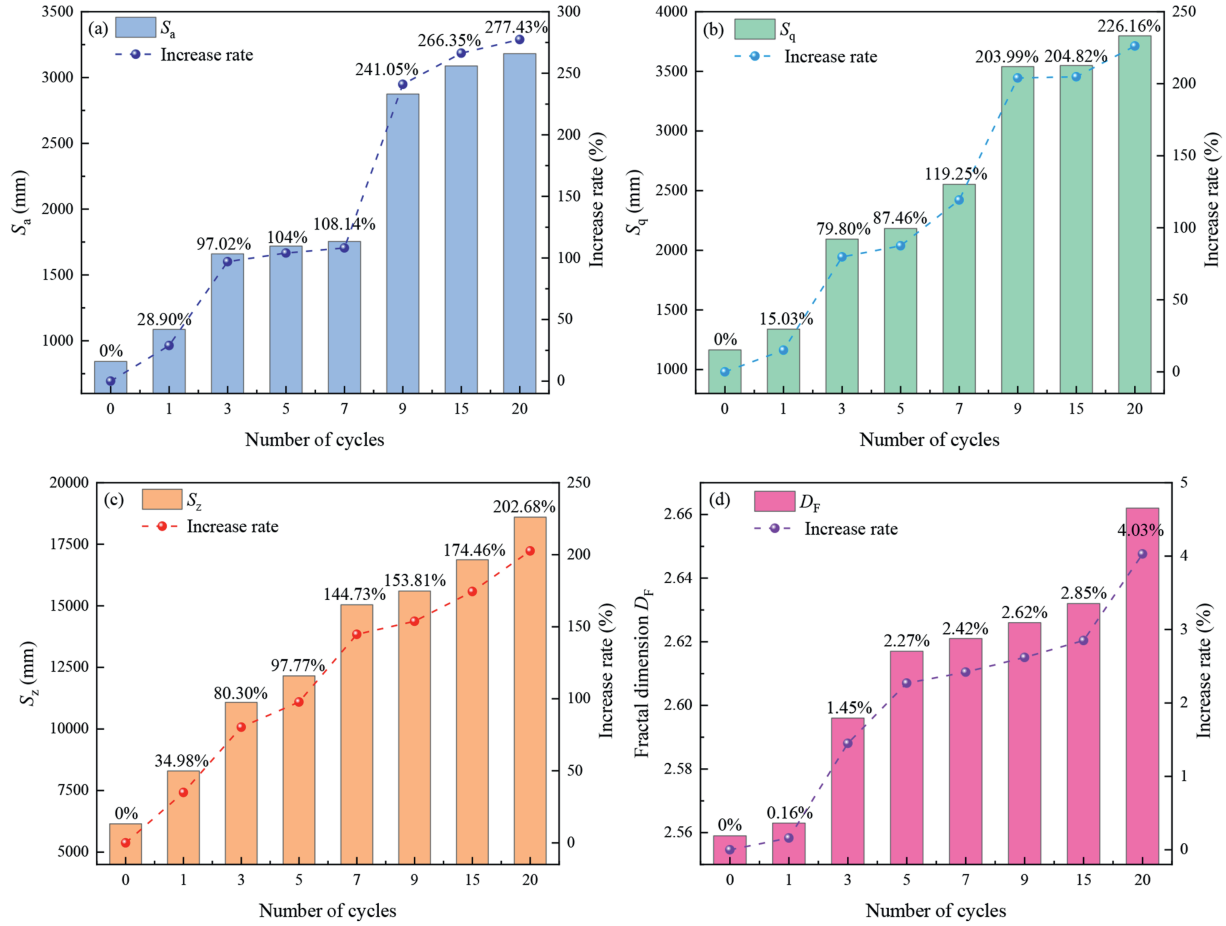

Fig. 22. Granite fracture surface roughness at different thermal cycles.

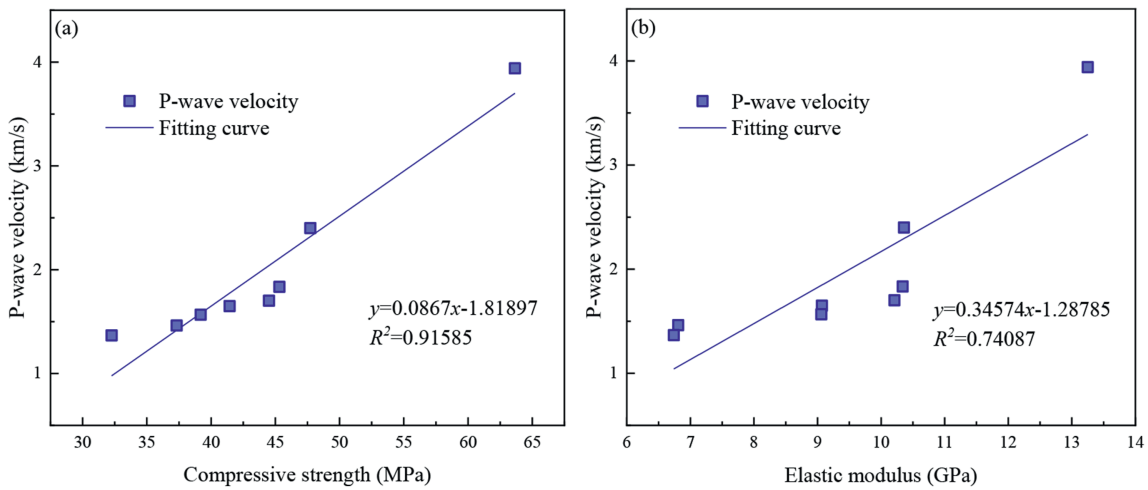

Fig. 23. Correlation between P-wave velocity and mechanical properties.

number of LN_2 cooling cycles increases, the mechanical properties of granite gradually deteriorate. To establish the relationship between various parameters (such as compressive strength, elastic modulus, P-wave velocity, and amplitude) and cycle numbers, we performed regression analysis using polynomial, power, and exponential function models. Table 1 presents the regression results of different mathematical models. The results show that the exponential function model has a higher correlation coefficient ($R^2 > 0.86$) and better describes the trend of mechanical parameters with respect to cycle numbers. Therefore, the empirical regression of mechanical parameters with cycle numbers can be expressed by the following equation:

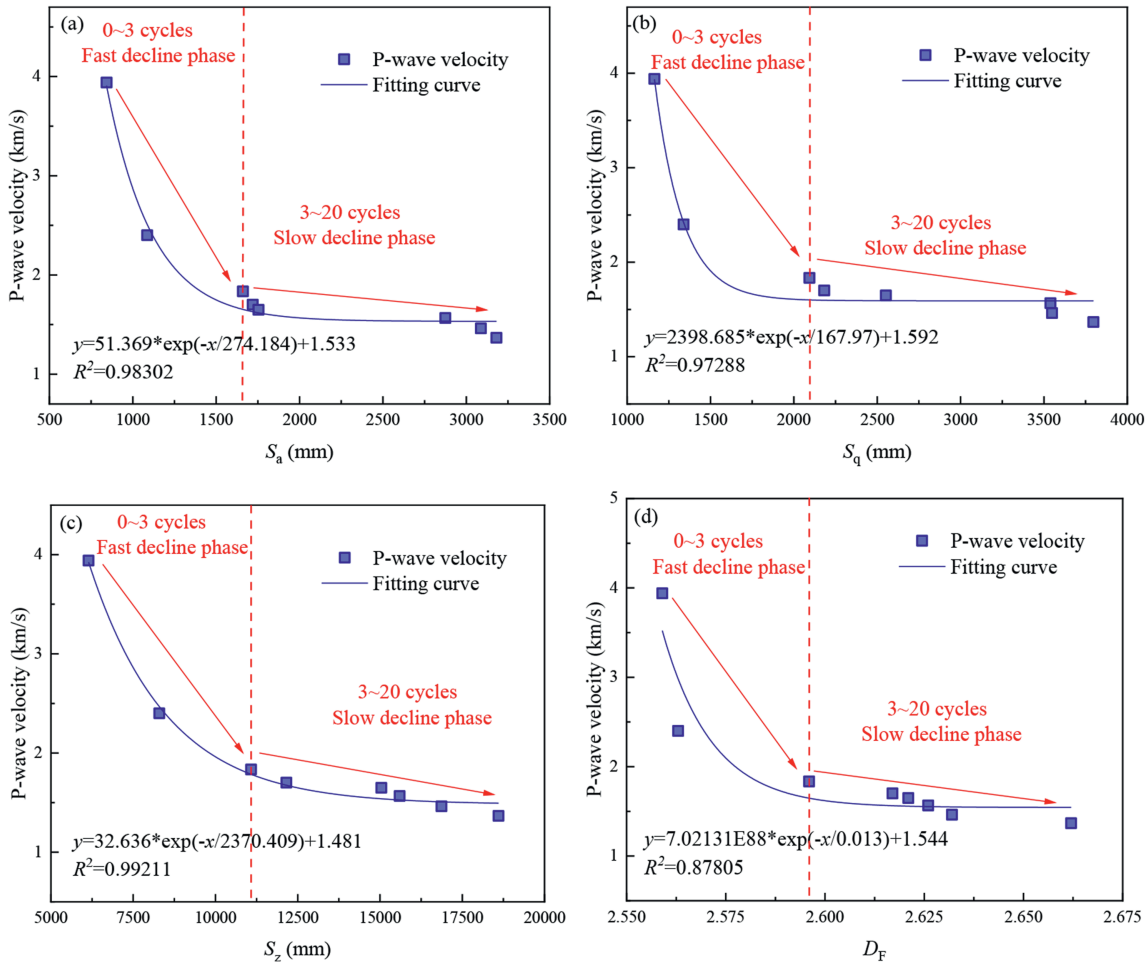

Fig. 24. Correlation between P-wave velocity and surface roughness.

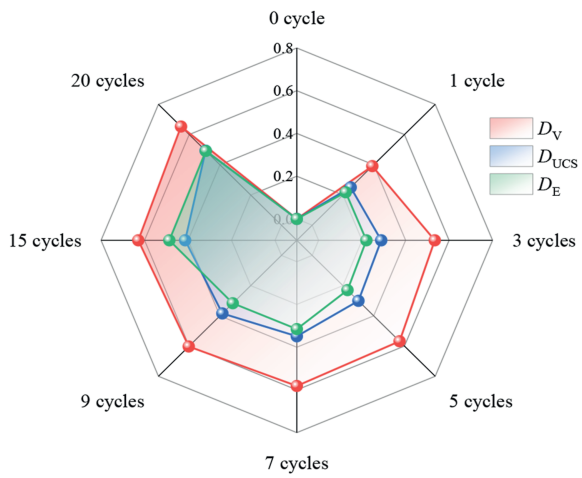

Fig. 25. Thermal damage assessment based on different mechanical properties.

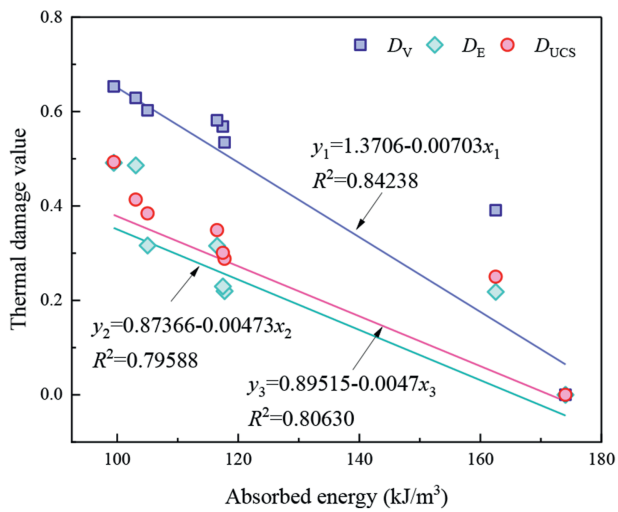

Fig. 26. Relationship between energy absorption and thermal damage value of granite.

$$y = ae^{(-x/b)} + c \tag{10}$$

where y represents the value of the mechanical parameter (such as compressive strength, elastic modulus, P-wave velocity, and amplitude), x represents the number of cycles, and a, b, and c are the fitting coefficients.

4.3. Mechanism of thermal damage

The mechanical behavior of granite at the macroscopic scale is fundamentally governed by changes in its microstructure. In fact,

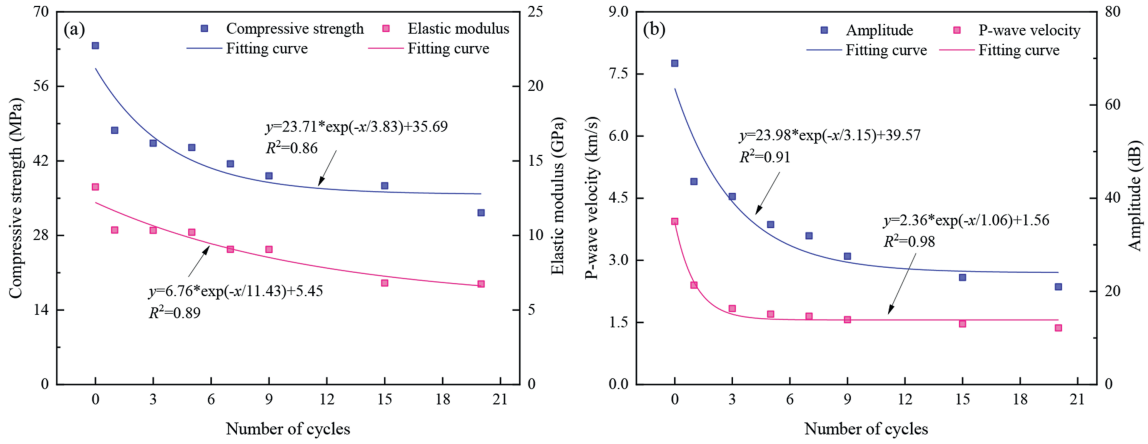

Fig. 27. Evolution of granite mechanical parameters with different cycle numbers.

Table 1
Regression results of different mathematical models.

Parameters	Polynomial model	Power model	Exponential model
Compressive strength	$y = 56.07–2.63x + 0.08x^2$, $R^2 = 0.81$	$y = 49.85x^{-0.11}$, $R^2 = 0.84$	$y = 23.71e^{(-x/3.83)} + 35.69$, $R^2 = 0.86$
Elastic modulus	$y = 12.12–0.50x + 0.01x^2$, $R^2 = 0.84$	$y = 11.27x^{-0.13}$, $R^2 = 0.68$	$y = 6.76e^{(-x/11.43)} + 5.45$, $R^2 = 0.89$
P-wave velocity	$y = 3.14–0.29x + 0.01x^2$, $R^2 = 0.73$	$y = 2.35x^{-0.19}$, $R^2 = 0.97$	$y = 2.36e^{(-x/1.06)} + 1.56$, $R^2 = 0.98$
Amplitude	$y = 57.74–5.03x + 0.17x^2$, $R^2 = 0.85$	$y = 46.46x^{-0.23}$, $R^2 = 0.89$	$y = 23.98e^{(-x/3.15)} + 39.57$, $R^2 = 0.91$

the microstructural damage of granite results from the interplay of multiple factors. Fig. 28 illustrates the damage mechanisms of granite during the thermal cycling involving high-temperature heating and LN_2-cooling. In the process of heating, differential thermal expansion of the different mineral phases in granite serves as the primary driver of microstructural damage (Hu et al., 2021). When granite is subjected to high temperatures, adjacent mineral phases undergo thermal expansion as the temperature increases. However, as a result of the minerals' differing thermal expansion coefficients, this results in misaligned deformation between the mineral grains, generating thermal stresses. Once these thermal stresses exceed the bonding strength between the grains, thermal cracks propagate along the grain boundaries. As the primary constituent of granite, quartz—characterized by its relatively large and variable expansion coefficient—contributes significantly to the development of thermal cracks (Kranz, 1983). It has been observed that at 573 °C, quartz transforms from α-quartz to β-quartz (Glover et al., 1995). When quartz is raised in temperature from ambient levels to 600 °C, its volume can increase by 4.6 %, whereas other minerals, such as feldspar, experience only a 1 %–2 % volume increase. As a result, the varying thermal expansion between mineral grains at elevated temperatures helps drive the propagation of microcracks (Simmons and Cooper, 1978).

Additionally, when the thermally treated granite samples come into contact with LN_2, the substantial temperature gradient between the two will induce intense thermal exchange. During this process, secondary thermal stresses are generated within the granite, as shown in Eq. (11) (Zhu et al., 2019).

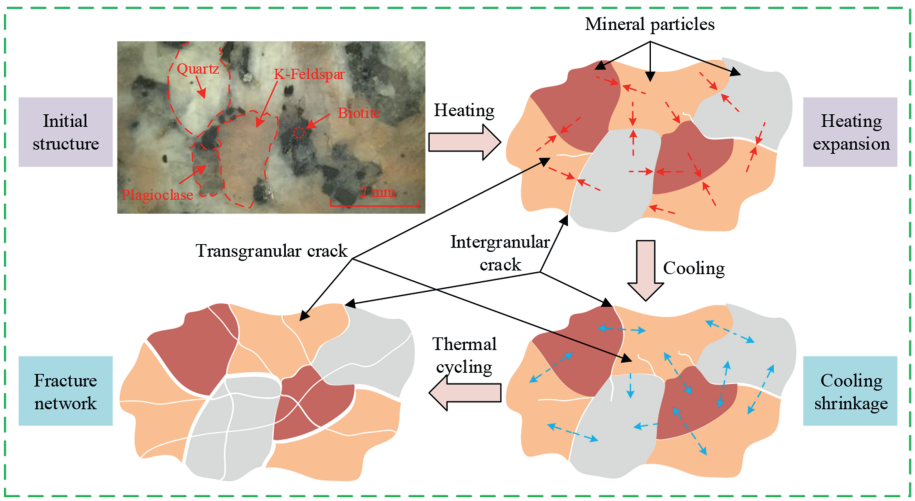

Fig. 28. Damage mechanisms of granite during heating and LN_2-cooling cycles.

$$\sigma_{ij} = E_{ij}\varepsilon_{ij} = \frac{E_{ij}\alpha_{ij}\Delta T_{ij}}{1-2\nu_{ij}} \tag{11}$$

where σ_{ij} represents the secondary thermal stress, α_{ij} is the thermal expansion coefficient, E_{ij} denotes the modulus of elasticity, ν_{ij} is the Poisson's ratio, ε_{ij} stands for the strain, and ΔT_{ij} is the temperature gradient.

As shown in Fig. 28, during the rapid cooling of granite with LN_2, transient thermal stresses manifest as tensile stresses on the rock surface. Usually, the compressive strength of granite exceeds its tensile strength. Consequently, microcracks induced by tensile stresses, under LN_2-cooling, are the primary contributors to the deterioration of granite's mechanical properties. It is crucial to highlight that the decline in granite's physico-mechanical properties following multiple cycles of high-temperature heating and LN_2-cooling does not follow a linear pattern. This indicates that the magnitude of thermal stresses generated in each cycle varies, indicating a correlation between the induced secondary thermal stresses and the number of cycles. At low cycle counts, the uneven deformation of mineral grains leads to the initiation of microcracks, with some intergranular cracks propagating along the mineral boundaries. As the number of cycles continues to rise, the cracks formed during the initial cycles alleviate localized stress concentrations, thus minimizing the creation of new microcracks. Therefore, the mechanical properties of the granite no longer exhibit a significant decline. However, the secondary thermal stresses induced by multiple cycles further exacerbate the stress concentration at the crack tips, promoting the propagation and coalescence of pores and fractures, thereby significantly enhancing the fracturability of the granite.

5. Conclusions

This research involved conducting physical-mechanical tests and analyzing the surface morphology of granite after exposure to cycles of high-temperature heating and LN_2-cooling. The ultrasonic properties, fracture behavior, and crack evolution of the granite were investigated. The formation mechanisms and evolutionary characteristics of macro- and micro-cracks in granite under different cycle counts were analyzed. Additionally, the damage mechanisms and fracturability of high-temperature granite treated with LN_2 cycles were explored. The key conclusions are as follows:

(1) High-temperature heating and LN_2-cooling cycles induce significant structural damage to granite. The number of cycles correlates with a marked decrease in P-wave velocity, amplitude, compressive strength, elastic modulus, and fracture energy. Additionally, the regularity and integrity of the ultrasonic waveforms are diminished, with a reduction in the initial, central, and tail wave amplitudes. The P-wave velocity and amplitude decrease by 53.45 % and 40.55 %, respectively. The bandwidth of the secondary frequency band decreases and gradually converges to the main frequency band, while the width of the main frequency band increases. The repeated high-temperature heating and LN_2-cooling cycles cause an increase in the quantity and size of microcracks, leading to greater diffraction and scattering of acoustic waves.

(2) The cyclic treatment alters the fracture morphology of the granite. Before the third cycle, the proportion of tensile microcracks exceeds that of shear microcracks. On a macroscopic scale, the fracture morphology of the granite develops along the axial direction, resulting in tensile cracks that are parallel to the axis. After 3 cycles, shear microcracks become dominant, and the primary fracture surface of the granite is characterized by oblique shear cracks. As the number of cycles increased, there was a corresponding rise in the quantity, depth, and tortuosity of the macroscopic cracks. Both shear and tensile cracks develop simultaneously, resulting in a complex fracture pattern.

(3) There is a positive correlation between the roughness parameters of granite and the number of cycles. After 20 cycles, the maximum increases in four roughness characteristic parameters of S_a, S_q, S_z, and D_F are 277.43 %, 226.16 %, 202.68 %, and 4.03 %, respectively. The combined effect of high-temperature heating and LN_2-cooling leads to significant changes in the fracture surface. During the high-temperature heating, the granite expands and becomes more brittle, while the subsequent rapid cooling with LN_2 causes thermal shock, inducing micro-fractures and increasing surface roughness. As the cycles progress, the fracture surface develops pronounced undulations, with stepped features becoming increasingly noticeable. Compared to a single cooling cycle, repeated LN_2-cooling is more likely to induce the formation of a large-scale and complex crack network.

(4) The LN_2 cycling treatment consists of two stages. From 0 to 3 cycles, the high-temperature heating and LN_2-cooling generate numerous thermally-induced cracks, which rapidly deteriorate the mechanical properties of granite and reduce the fracture initiation pressure. Between 3 cycles and 20 cycles, the number of newly formed cracks gradually decreases, and the mechanical properties deteriorate at a slower rate. The cycling cooling treatment increases the crack propagation paths, enhances the connectivity between cracks, and improves the fracturability of granite, which is beneficial for geothermal energy extraction.

CRediT authorship contribution statement

Yi Xue: Writing – original draft, Software, Conceptualization. **Linchao Wang:** Writing – original draft, Conceptualization. **Zhengzheng Cao:** Writing – original draft, Validation, Software, Resources. **Heping Xie:** Software, Formal analysis, Conceptualization. **P.G. Ranjith:** Writing – original draft, Validation, Conceptualization. **Chengzheng Cai:** Writing – original draft, Conceptualization.

Declaration of competing interest

The authors declare that they have no known competing financial interests or personal relationships that could have appeared to influence the work reported in this paper.

Acknowledgments

The authors are grateful for the financial support from the National Natural Science Foundation of China (Grant No. 52274096).

References

Al-Ameri, N.J., Hamd-Allah, S.M., 2023. Sonic scanner helps in identifying reservoir potential and isotropic characteristics of Khasib formation. Iraqi J. Geol. 129–143.

Asai, P., Podgorney, R., McLennan, J., Deo, M., Moore, J., 2022. Analytical model for fluid flow distribution in an Enhanced Geothermal Systems (EGS). Renew. Energy 193, 821–831.

Breede, K., Dzebisashvili, K., Liu, X., Falcone, G., 2013. A systematic review of enhanced (or engineered) geothermal systems: past, present and future. Geotherm. Energ. 1 (1), 1–27.
Cha, M., Alqahtani, N.B., Yin, X., Wang, L., Yao, B., Kneafsey, T.J., Wu, Y.S., 2021. Propagation of cryogenic thermal fractures from unconfined Pmma boreholes. Energies 14 (17), 5433.
Chen, C., Lou, Z.H., Jin, A.M., 2017. Acoustic anisotropy of water-saturated and desiccated carbonate rocks. Lithol. Reserv. 29, 131–137.
Chen, Z., He, C., Ma, G., Xu, G., Ma, C., 2019. Energy damage evolution mechanism of rock and its application to brittleness evaluation. Rock Mech. Rock Eng. 52 (4), 1265–1274.
Du, K., Li, X., Tao, M., Wang, S., 2020. Experimental study on acoustic emission (AE) characteristics and crack classification during rock fracture in several basic lab tests. Int. J. Rock Mech. Min. Sci. 133, 104411.
Fan, L., Li, H., Xi, Y., 2022. Evaluation of the effects of three different cooling methods on the dynamic mechanical properties of thermal-treated sandstone. Bull. Eng. Geol. Environ. 81 (4), 154.
Ge, Z., Sun, Q., 2018. Acoustic emission (AE) characteristics of granite after heating and cooling cycles. Eng. Fract. Mech. 200, 418–429.
Ge, Z., Sun, Q., Yang, T., Luo, T., Jia, H., Yang, D., 2021. Effect of high temperature on mode-I fracture toughness of granite subjected to liquid nitrogen cooling. Eng. Fract. Mech. 252, 107834.
Glover, P.W.J., Baud, P., Darot, M., Meredith, P., Boon, S.A., LeRavalec, M., Reuschlé, T., 1995. α/β phase transition in quartz monitored using acoustic emissions. Geophys. J. Int. 120 (3), 775–782.
Hamd-Allah, S.M., Al-Ameri, N.J., 2023. Investigating tight oil reservoir production performance: influence of geomechanical parameters and their distribution. Petrol. Res. 8 (4), 490–498.
Hong, C., Yang, R., Huang, Z., Qin, X., Wen, H., Cong, R., Chen, J., 2022. Fracture initiation and morphology of tight sandstone by liquid nitrogen fracturing. Rock Mech. Rock Eng. 55 (3), 1285–1301.
Hou, P., Su, S., Liang, X., Gao, F., Cai, C., Yang, Y., Zhang, Z., 2021. Effect of liquid nitrogen freeze–thaw cycle on fracture toughness and energy release rate of saturated sandstone. Eng. Fract. Mech. 258, 108066.
Hu, J., Sun, Q., Pan, X., 2018. Variation of mechanical properties of granite after high-temperature treatment. Arab. J. Geosci. 11 (2), 43.
Hu, J., Xie, H., Gao, M., Li, C., Sun, Q., 2022. Damage mechanism and heat transfer characteristics of limestone after thermal shock cycle treatments based on geothermal development. Int. J. Rock Mech. Min. Sci. 160, 105269.
Hu, J., Xie, H., Sun, Q., Li, C., Liu, G., 2021. Changes in the thermodynamic properties of alkaline granite after cyclic quenching following high temperature action. Int. J. Min. Sci. Technol. 31 (5), 843–852.
Jamshidi, A., Zamanian, H., Zarei Sahamieh, R., 2018. The effect of density and porosity on the correlation between uniaxial compressive strength and P-wave velocity. Rock Mech. Rock Eng. 51 (4), 1279–1286.
Jia, Y., Lu, Y., Elsworth, D., Fang, Y., Tang, J., 2018. Surface characteristics and permeability enhancement of shale fractures due to water and supercritical carbon dioxide fracturing. J. Petrol. Sci. Eng. 165, 284–297.
Kranz, R.L., 1983. Microcracks in rocks: a review. Tectonophysics 100 (1), 449–480.
Li, Q., Yin, T., Li, X., Zhang, S., 2020. Effects of rapid cooling treatment on heated sandstone: a comparison between water and liquid nitrogen cooling. Bull. Eng. Geol. Environ. 79 (1), 313–327.
Li, W., Fang, S., Gao, X., Han, Y., 2023. Method of defining rock damage variable on the basis of wave impedance. Energ. Sci. Eng. 11 (10), 3641–3661.
Lü, C., Sun, Q., Zhang, W., Geng, J., Qi, Y., Lu, L., 2017. The effect of high temperature on tensile strength of sandstone. Appl. Therm. Eng. 111, 573–579.
Lu, S.M., 2018. A global review of enhanced geothermal system (EGS). Renew. Sustain. Energ. Rev. 81, 2902–2921.
Mahesar, A.A., Ali, M., Shar, A.M., Memon, K.R., Mohanty, U.S., Akhondzadeh, H., Keshavarz, A., 2020. Effect of cryogenic liquid nitrogen on the morphological and petrophysical characteristics of tight gas sandstone rocks from kirthar fold belt, Indus Basin, Pakistan. Energ. Fuels 34 (11), 14548–14559.
Mansurov, V.A., 1994. Acoustic emission from failing rock behaviour. Rock Mech. Rock Eng. 27 (3), 173–182.
Pappalardo, G., 2015. Correlation between P-wave velocity and physical–mechanical properties of intensely jointed dolostones, Peloritani mounts, NE Sicily. Rock Mech. Rock Eng. 48 (4), 1711–1721.
Qu, H., Tang, S., Liu, Y., Huang, P., Wu, X., Liu, Z., Li, C., 2022. Characteristics of complex fractures by liquid nitrogen fracturing in brittle shales. Rock Mech. Rock Eng. 55 (4), 1807–1822.
Rong, G., Sha, S., Li, B., Chen, Z., Zhang, Z., 2021. Experimental investigation on physical and mechanical properties of granite subjected to cyclic heating and liquid nitrogen cooling. Rock Mech. Rock Eng. 54 (5), 2383–2403.
Sang, G., Liu, S., Elsworth, D., 2020. Quantifying fatigue-damage and failure-precursors using ultrasonic coda wave interferometry. Int. J. Rock Mech. Min. Sci. 131, 104366.
Sha, S., Rong, G., Chen, Z., Li, B., Zhang, Z., 2020. Experimental evaluation of physical and mechanical properties of geothermal reservoir rock after different cooling treatments. Rock Mech. Rock Eng. 53, 4967–4991.
Shao, Z., Sun, L., Aboayanah, K.R., Liu, Q., Grasselli, G., 2022. Investigate the mode I fracture characteristics of granite after heating/-LN_2 cooling treatments. Rock Mech. Rock Eng. 55 (7), 4477–4496.
Sharma, P.K., Singh, T.N., 2008. A correlation between P-wave velocity, impact strength index, slake durability index and uniaxial compressive strength. Bull. Eng. Geol. Environ. 67 (1), 17–22.
Simmons, G., Cooper, H.W., 1978. Thermal cycling cracks in three igneous rocks. Int. J. Rock Mech. Min. Sci. Geomech. Abstr. 15 (4), 145–148.
Su, S., Hou, P., Gao, F., Liang, X., Ding, R., Cai, C., 2022. Changes in mechanical properties and fracture behaviors of heated marble subjected to liquid nitrogen cooling. Eng. Fract. Mech. 261, 108256.
Sun, Q., Zhang, W., Xue, L., Zhang, Z., Su, T., 2015. Thermal damage pattern and thresholds of granite. Environ. Earth Sci. 74 (3), 2341–2349.
Sun, Y., Zhai, C., Xu, J., Cong, Y., Zheng, Y., 2021. Experimental study on pore structure evolution of coal in macroscopic, mesoscopic, and microscopic scales during liquid nitrogen cyclic cold-shock fracturing. Fuel 291, 120150.
Sun, Y., Zhai, C., Xu, J., Yu, X., Cong, Y., Zheng, Y., Li, Y., 2022. Damage and failure of hot dry rock under cyclic liquid nitrogen cold shock treatment: a non-destructive ultrasonic test method. Nat. Resour. Res. 31 (1), 261–279.
Wang, H., Liu, D., Cui, Z., Cheng, C., Jian, Z., 2016. Investigation of the fracture modes of red sandstone using XFEM and acoustic emissions. Theor. Appl. Fract. Mech. 85, 283–293.
Wang, L., Zhu, L., Cao, Z., Liu, J., Xue, Y., Wang, P., Liu, Y., 2025. Thermo-mechanical degradation and fracture evolution in low-permeability coal subjected to cyclic heating–cryogenic cooling. Phys. Fluids 37 (8), 086617.
Wang, Y., Hou, P., Su, S., Liang, X., Gao, F., Gao, Y., Liu, Q., 2024. Experimental study on mode I fracture characteristics of heated granite subjected to water and liquid nitrogen cooling treatments. Eng. Fract. Mech. 298, 109932.
Wanniarachchi, W.A.M., Ranjith, P.G., Perera, M.S.A., Rathnaweera, T.D., Lyu, Q., Mahanta, B., 2017. Assessment of dynamic material properties of intact rocks using seismic wave attenuation: an experimental study. R. Soc. Open Sci. 4 (10), 170896.
Wu, X., Huang, Z., Song, H., Zhang, S., Cheng, Z., Li, R., Dai, X., 2019. Variations of physical and mechanical properties of heated granite after rapid cooling with liquid nitrogen. Rock Mech. Rock Eng. 52 (7), 2123–2139.
Xi, Y., Wang, H., Jiang, J., Fan, L., Li, J., Guo, B., 2023. Impacts of different cooling methods on the dynamic tensile properties of thermal-treated granite. Int. J. Rock Mech. Min. Sci. 169, 105438.
Yin, T., Li, Q., Li, X., 2019. Experimental investigation on mode I fracture characteristics of granite after cyclic heating and cooling treatments. Eng. Fract. Mech. 222, 106740.
Zhang, W., Sun, Q., Hao, S., Geng, J., Lv, C., 2016. Experimental study on the variation of physical and mechanical properties of rock after high temperature treatment. Appl. Therm. Eng. 98, 1297–1304.
Zheng, K., Wang, C., Zhao, Y., Bi, J., 2023. Theoretical and experimental researches on fracture toughness for bedded shale using the centrally cracked Brazilian disk method with acoustic emission monitoring. Theor. Appl. Fract. Mech. 124, 103784.
Zhu, C., Peng, S., Zhou, X., Zhu, X., Qiao, J., Yan, L., Li, X., Shi, W., 2025. Compacting effect study on the treatment of collapsible loess foundation by the SDDC method: numerical and experimental analysis. Int. J. Numer. Anal. Methods GeoMech. 49 (11), 2529–2548.
Zhu, L., Yu, J., Gao, H., Gang, L., Zhou, X., Zheng, X., 2019. Effect of water cooling on microscopic damage and dynamic properties of high-temperature granite. Explos. Shock Waves 39 (8), 083104.

Dr. Yi Xue is an Associate Professor at the Geotechnical Institute of Xi'an University of Technology, China. He received his BSc and PhD degrees from the State Key Laboratory for Geomechanics and Deep Underground Engineering, China University of Mining and Technology. In 2017, he was honored with the Excellent Doctoral Dissertation Award by the Chinese Society for Rock Mechanics and Engineering. He has published more than 100 scientific papers, with research interests covering rock seepage theory, multi-field coupling theory, intelligent rock mechanics, and geothermal resource development. He is a council member of the Shaanxi Society for Rock-Soil Mechanics and Engineering and serves on its Youth Committee. In 2021, he was selected for the Youth Talent Promotion Program of the Xi'an Association for Science and Technology. He has led several research projects funded by the National Natural Science Foundation of China, the Special Support of the China Postdoctoral Science Foundation, and the Special Support of the Shaanxi Postdoctoral Research Project.